



# Assessment of Closed Loop Mode Performance and Feasibility of an Open Loop Mode for SARin missions

## Impact Assessment Reports (Inland Water)

For the attention of: Mr. David COTTON, SatOC  
Mr. Jérôme BENVENISTE, ESRIN/ESA  
Mr. Marco RESTANO, ESRIN/ESA

	Function	Name	Signature	Date
Prepared by	Project manager/ Project Team	Alexandre HOMERIN		21/03/23
Approved by	Deputy CEO	Mahmoud EL HAJJ		21/03/23



<b>ASSESSMENT OF CLOSED LOOP MODE PERFORMANCE AND FEASIBILITY OF AN OPEN LOOP MODE FOR SARIN MISSIONS</b>	Ref	NOV-FE-0747-NT-013		
	Issue	1	Date	21/03/23
	Rev	0	Date	21/03/23
	Page	3/36		

## ***Distribution list***

<b>INTERNAL</b>	<b>EXTERNAL</b>	
<b>Name</b>	<b>Name</b>	<b>Company / Organisation</b>
Documentation NOVELTIS	Mr. David COTTON, SatOC	SatOC
Richard BRU	Mr. Jérôme BENVENISTE	ESA
Project Team	Mr. Marco RESTANO	ESA



<b>ASSESSMENT OF CLOSED LOOP MODE PERFORMANCE AND FEASIBILITY OF AN OPEN LOOP MODE FOR SARIN MISSIONS</b>	Ref	NOV-FE-0747-NT-013		
	Issue	1	Date	21/03/23
	Rev	0	Date	21/03/23
	Page	5/36		

## *Acronyms*

CL	Closed-Loop
DEM	Digital Elevation Model
JRC	Joint Research Centre
LRM	Low Resolution Measurement
OLTC	Open Loop Tracking Command
POCA	Point Of Closest Approach
SNR	Signal to Noise Ratio
SAR	Synthetic-Aperture Radar
SARin	Interferometric Synthetic-Aperture Radar
SIRAL	SAR Interferometric Radar Altimeter
SRAL	SAR Radar Altimeter (Sentinel-3)

## References

[RD1]	Martin-Puig, C., Leuliette, E., Lillibridge, J., & Roca, M. (2016). Evaluating the Performance of Jason-2 Open-Loop and Closed-Loop Tracker Modes, <i>Journal of Atmospheric and Oceanic Technology</i> , 33(11), 2277-2288. Retrieved Mar 21, 2022, from <a href="https://journals.ametsoc.org/view/journals/atot/33/11/jtech-d-16-0011_1.xml">https://journals.ametsoc.org/view/journals/atot/33/11/jtech-d-16-0011_1.xml</a>
[RD2]	Le Gac, Sophie; Boy, François; Blumstein, Denis; Lasson, Léa; Picot, Nicolas (2019). <i>Benefits of the Open-Loop Tracking Command (OLTC): Extending conventional nadir altimetry to inland waters monitoring</i> . <i>Advances in Space Research</i> , (), S0273117719307811. doi:10.1016/j.asr.2019.10.031
[RD3]	D.J. Wingham; C.R. Francis; S. Baker; C. Bouzinac; D. Brockley; R. Cullen; P. de Chateau-Thierry; S.W. Laxon; U. Mallow; C. Mavrocordatos; L. Phalippou; G. Ratier; L. Rey; F. Rostan; P. Viau; D.W. Wallis (2006). <i>CryoSat: A mission to determine the fluctuations in Earth's land and marine ice fields</i> , 37(4), 841–871. doi:10.1016/j.asr.2005.07.027
[RD4]	ESA. CRYOSAT Ground Segment Instrument Processing Facility L2. <i>CryoSat Ice netCDF L2 Product Format Specification</i> . Published online July 14, 2021. <a href="https://earth.esa.int/eogateway/documents/20142/37627/CryoSat-netCDF-L2-Product-Format-Specification.pdf">https://earth.esa.int/eogateway/documents/20142/37627/CryoSat-netCDF-L2-Product-Format-Specification.pdf</a>
[RD5]	ESA. CRYOSAT Ground Segment Instrument Processing Facility L1B. <i>CryoSat Ice netCDF L1B Product Format Specification</i> . Published online December 23, 2020. <a href="https://earth.esa.int/eogateway/documents/20142/37627/CryoSat-netCDF-L1b-Product-Format-Specification.pdf">https://earth.esa.int/eogateway/documents/20142/37627/CryoSat-netCDF-L1b-Product-Format-Specification.pdf</a>
[RD6]	ESA. Cryosat-2 Product Handbook. Published online April 3, 2018. <a href="https://earth.esa.int/eogateway/documents/20142/37627/cryosat-baseline-d-product-handbook/f28680ea-13de-c7e1-884a-d273b8945905?version=1.0&amp;download=true">https://earth.esa.int/eogateway/documents/20142/37627/cryosat-baseline-d-product-handbook/f28680ea-13de-c7e1-884a-d273b8945905?version=1.0&amp;download=true</a>
[RD7]	Berry, P. A. M., Smith, R., & Benveniste, J. (2018). Altimeter Corrected Elevations, Version 2 (ACE2) [Data set]. Palisades, NY: NASA Socioeconomic Data and Applications Center (SEDAC). <a href="https://doi.org/10.7927/H40G3H78">https://doi.org/10.7927/H40G3H78</a>
[RD8]	Lehner, B., & Messenger, M. (2016, décembre). HydroLAKES Technical Documentation Version 1.0. Department of Geography, McGill University Montreal, Quebec, Canada.
[RD9]	Joint Research Centre. (2020). <i>Global Surface Water - Data Users Guide (v3)</i> . Copernicus Program.
[RD10]	Global Surface Water - Data Access. (2021). Global Surface Water Explorer. <a href="https://global-surface-water.appspot.com/download">https://global-surface-water.appspot.com/download</a>
[RD11]	EU-Hydro - River Network Database — Copernicus Land Monitoring Service. (2022). Copernicus. <a href="https://land.copernicus.eu/imagery-in-situ/eu-hydro/eu-hydro-river-network-database?tab=metadata">https://land.copernicus.eu/imagery-in-situ/eu-hydro/eu-hydro-river-network-database?tab=metadata</a>
[RD12]	Gallaun, H., Dohr, K., M.P., Stumpf, A., & Hugé, J. (2020). EU-Hydro - River Net User Guide 1.3. European Environment Agency. <a href="https://land.copernicus.eu/user-corner/technical-library/eu-hydro_user_guide.pdf">https://land.copernicus.eu/user-corner/technical-library/eu-hydro_user_guide.pdf</a>
[RD13]	ESA. (2012). CUT Software Administrator and Operator Manual. <a href="https://earth.esa.int/eogateway/documents/20142/1088833/CUT-SAOM-1.3.pdf">https://earth.esa.int/eogateway/documents/20142/1088833/CUT-SAOM-1.3.pdf</a>
[RD14]	CRISTAL orbit new candidates – The Polar Monitoring Project. (s. d.). <a href="https://www.polarmonitoringproject.org/cristal-orbit-new-candidates/">https://www.polarmonitoringproject.org/cristal-orbit-new-candidates/</a>

<b>ASSESSMENT OF CLOSED LOOP MODE PERFORMANCE AND FEASIBILITY OF AN OPEN LOOP MODE FOR SARIN MISSIONS</b>	Ref	NOV-FE-0747-NT-013		
	Issue	1	Date	21/03/23
	Rev	0	Date	21/03/23
	Page	7/36		

## *Table of contents*

<b>1. INTRODUCTION</b>	<b>9</b>
<b>2. DATA AND PRODUCTS</b>	<b>10</b>
2.1. CRYOSAT-2 ALTIMETRY DATA	10
2.2. AREA OF INTEREST	11
2.3. ELEVATION REFERENCES	11
2.4. OTHER DATASETS	13
2.4.1. <i>HydroLakes database for lakes</i>	13
2.4.2. <i>River contours</i>	13
<b>3. GENERAL DIAGNOSTICS ON THE ZONE OF INTEREST</b>	<b>16</b>
3.1. DATA QUALITY	16
3.2. BIASES	17
<b>4. CASE STUDY: LAKE GENEVA</b>	<b>22</b>
4.1. COMPARING UNFLAGGED AND FLAGGED WAVEFORMS	23
4.2. COMPARING MEASUREMENTS OVER SUCCESSIVE CYCLES	26
4.2.1. <i>Relative orbit number 4128</i>	26
4.2.2. <i>Relative orbit number 167</i>	27
<b>5. DETECTING RIVERS IN MOUNTAINOUS AREAS</b>	<b>31</b>
<b>6. CONCLUSION</b>	<b>36</b>





<b>ASSESSMENT OF CLOSED LOOP MODE PERFORMANCE AND FEASIBILITY OF AN OPEN LOOP MODE FOR SARIN MISSIONS</b>	Ref	NOV-FE-0747-NT-013		
	Issue	1	Date	21/03/23
	Rev	0	Date	21/03/23
	Page	9/36		

# 1. Introduction

---

Radar altimeters provide accurate range measurement between the instrument and the surface, based on the return travel time of the emitted microwave signal. The range estimation results from on-board operations (tracking) and on-ground post-processing (retracking) of the received waveform. The latter is acquired in the altimeter reception window, which has a limited range size by design. Therefore, centering this window on a value close to the effective range is fundamental to receive quality radar echoes.

Altimeter tracking systems usually operate in two steps. First, during the *acquisition* phase, it looks for the backscattered signal received by the altimeter. Then, during the *tracking* phase, the signal position is locked after compensation for height rate variability and preservation of an adequate Signal to Noise Ratio (SNR). Altimeter tracking systems are designed to operate in an autonomous closed loop system. In this mode, the range window adjustment before the acquisition phase is based on the previous estimates of height and height rate. This tracking system is efficient to track the elevation of relatively flat surfaces with no abrupt elevation jump. It works very well to measure the ocean levels, which is the primary intent of space altimetry missions such as the Jason series or the Sentinel-3 constellation.

After several years of ocean level measurements with an improved accuracy through space altimetry, the possibility of retrieving water surface height with the same space altimeters was investigated. However, tracking a wide variety of water bodies (rivers, lakes, reservoirs, wetlands) in diverse environments (mountainous areas with sudden topography changes, seasonality of weather conditions such as ice coverage) presents different constraints from those associated with the measurements of our ocean elevations. [RD1] highlighted that the closed loop tracking system shows poor performances when measuring inland water levels, especially in areas with large height variability, where the tracker often loses track.

In order to improve the performances over inland waters without degrading the accuracy over oceans, the Open Loop Tracking Command (OLTC) was introduced. This solution consists in controlling the reception window position with an on-board “pseudo” Digital Elevation Model, which gives an “a priori” information on the overflown surface elevation. This tracking mode has been implemented onboard the Jason-2, SARAL/AltiKa, Jason-3, Sentinel-3 A and B and Sentinel-6A satellites and has demonstrated excellent performances over continental water bodies [RD2]. In particular, this reference demonstrated that half of the inland water bodies measured by Jason-3 in OL mode were never captured in autonomous (CL) mode. The performance of the OLTC mode is such that it is now stated as operational mode for Jason-3, S3A&B and S6A. A key factor of the OLTC success is the quality of the input database used to generate the OLTC. Without precise a priori information, the reception window will miss the backscattered echo.

Until now the use of the OLTC has been restricted to conventional nadir altimetry (LRM, SAR) missions. SARin missions such as CryoSat-2 are still currently operated in CL mode [RD3]. In this report we will show that the current tracking mode has limitations when it comes to measuring inland water levels, and we will investigate the possibility for an OLTC implementation to improve the performance.

Ref	NOV-FE-0747-NT-013		
Issue	1	Date	21/03/23
Rev	0	Date	21/03/23
Page	10/36		

## 2. Data and products

### 2.1. CryoSat-2 altimetry data

CryoSat-2’s primary payload is the SAR/Interferometric Radar Altimeter (SIRAL). Initially designed to measure ice sheet elevation and sea-ice freeboard, it is able to operate in three different modes: Low Resolution Mode (LRM), Synthetic Aperture Radar mode (SAR), and SAR interferometric mode (SARin). The first two modes constitute typical exploitation modes for nadir altimeters. The SARin mode allows for along-track aperture synthesis using two antennas and for phase comparison (interferometry) between the echoes received by each antenna. The earliest arrival of the echo at the satellite is from the point of closest approach (POCA). Then, based on this arrival time, the interferometer uses the phase difference between both antennas to determine the exact location of the POCA. This means that the received signal is tracked back to its origin. Water bodies usually reflect highly specular waveforms. As a consequence, such hydrological targets are likely to be dominant in the received echo, even if they are not located at nadir.

The SARin mode has the advantage of detecting water bodies located beside the satellite track, but the use of this mode may lead to a mis-ranging phenomenon. Energy from ambiguous beams can be interpreted by the ground processing chain as earliest echo arrival, or the across track angle (i.e. the POCA position) can be misinterpreted because of the phase wrapping of the interferometer phase. CryoSat-2 provides an “ambiguity check” to detect those potential errors by comparing the measured height with an elevation model of the surface. Unfortunately, as the CryoSat-2 SARin mode was designed to measure ice sheet elevations, the DEM used only covers Antarctica and Greenland.

The CryoSat-2 satellite orbits at an altitude of 717 km, with a 369-day period and an inclination of 92 degrees [RD3]]. Therefore, its ground track is quite dense, with a spacing of approximately 7-8 km at the Equator. The SIRAL instrument has a swath of approximately 14 km, and the SAR and SARin modes allow an along-track resolution of about 300 meters. The SARin mode operates following a geographical mask defined by ESA as shown on Figure 1.

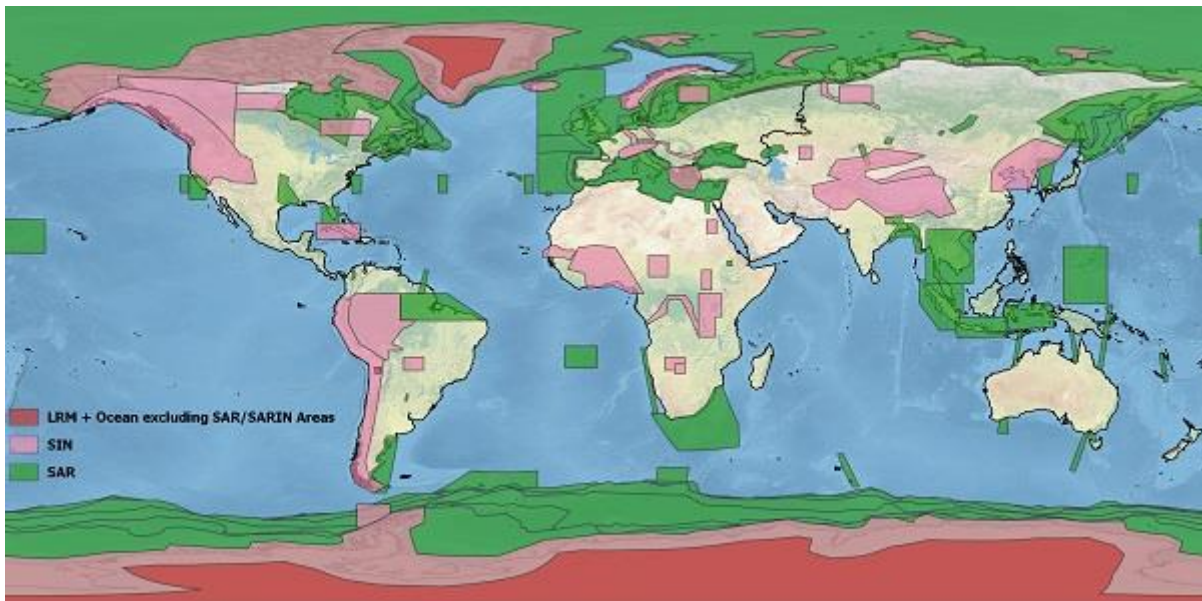


Figure 1: Cryosat Geographical Mode Masks (Version 4.0, latest release).

<https://earth.esa.int/eogateway/news/cryosat-geographical-mode-mask-4-0-released>

In the first instance, we use the Level 2 processed data of the CryoSat-2 ICE product (*SIR\_SIN12\_*, baseline D, product specifications in [RD4]), which notably contains the POCA heights and locations retracked from the waveforms received by the two antennas. It is important to note that the height given by the SARin L2 product is referenced to the WGS84 ellipsoid ([RD7][RD6]). The L2 data also provides the geoid elevation information, derived from the EGM96 geoid, sampled under the ground track [RD6]. In order to have a measurement consistent with other elevation information used as reference (most DEMs are referenced to a geoid), the geoid elevation needs to be subtracted from the measured

<b>ASSESSMENT OF CLOSED LOOP MODE PERFORMANCE AND FEASIBILITY OF AN OPEN LOOP MODE FOR SARIN MISSIONS</b>	Ref	NOV-FE-0747-NT-013		
	Issue	1	Date	21/03/23
	Rev	0	Date	21/03/23
	Page	11/36		

height. In the next chapters, we will refer to the corrected height (retracked height-geoid elevation) simply as “height”. The Level 1B waveforms (*SIR\_SIN\_1B*, product specifications in [RD5]) are also occasionally used for more accurate diagnoses on hydrological targets of interest. Products used for our analysis span the whole year 2019. The data is downloaded using the CUT (Cryosat User Tool) software [RD13]. The software allows the filtering of the products, based on time and area of interest.

## 2.2. Area of interest

We will focus our analysis on the Alps, as delimited by a SARin polygon in the CryoSat-2 geographical mode mask (see Figure 2). The Alps Mountain range is also an area with very large height variability, which makes it suitable to explore the SARin limitations in a heterogeneous environment. As a comparison, we also retrieved data from an area with low height variability, the West Siberian Lakes. Finally, in order to focus a part of our analysis on rivers, we retrieved data using the Danube mode mask.

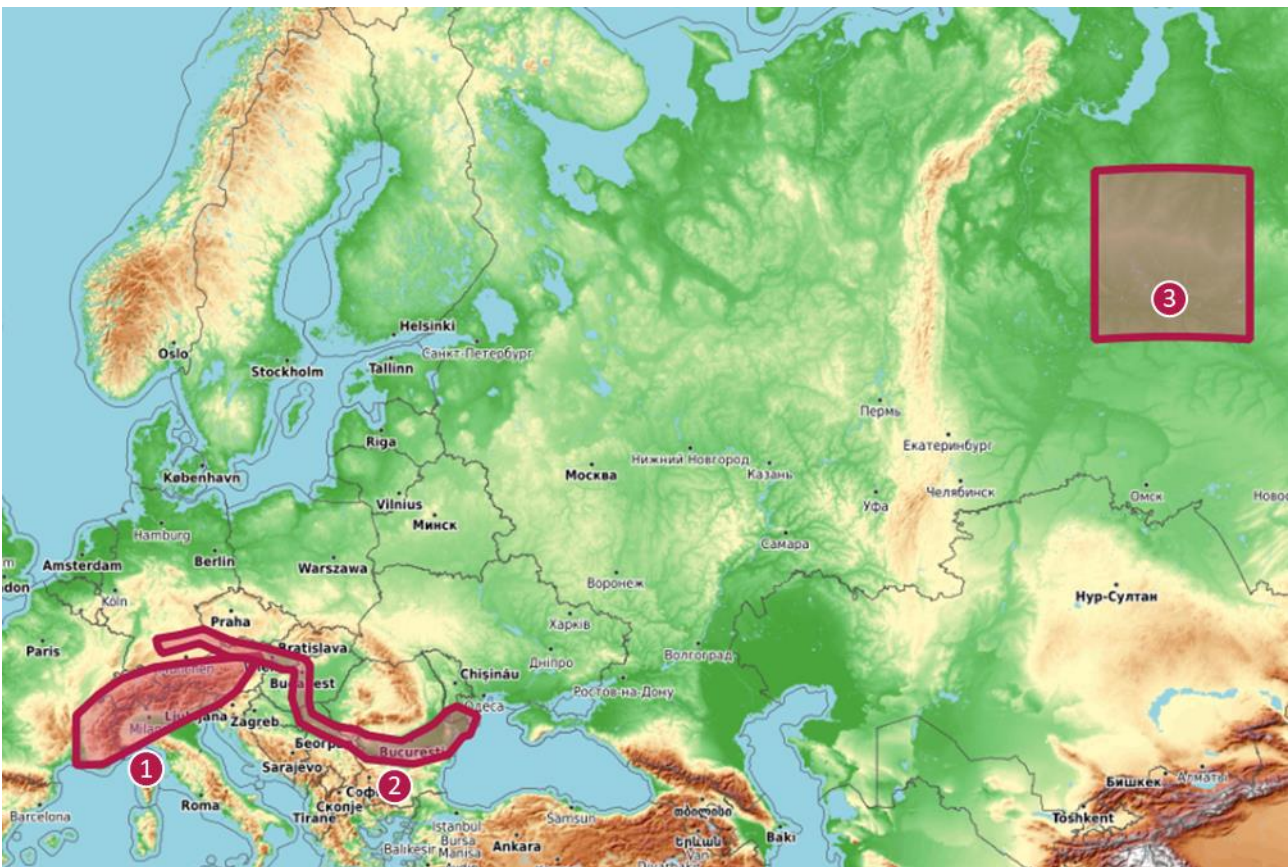


Figure 2: CryoSat-2 geographical SARin regions used. Names: 1) Alps, 2) Danube basin, 3) West Siberian Lakes

## 2.3. Elevation references

The accuracy of CryoSat-2 measurements will be evaluated with respect to an elevation reference. We used the global digital elevation model (GDEM) ACE2, which stands for Altimeter Corrected Elevation version 2. It was created by merging data from multiple satellite radar altimetry missions including the Shuttle Radar Topography Mission (SRTM). ACE2 is available globally at a spatial resolution of 3 arc-seconds (approximately 90 meters). This resolution is sufficient considering the 300m CryoSat-2 spatial sampling. However, the lake levels in ACE2 are derived from altimetry, and patched in the DEM at a resolution coarser than 90 meters (a few hundred meters). The GDEM reference ellipsoid is WGS84 and the geoid is EGM96 (specifications and user guides can be found in [RD7]).

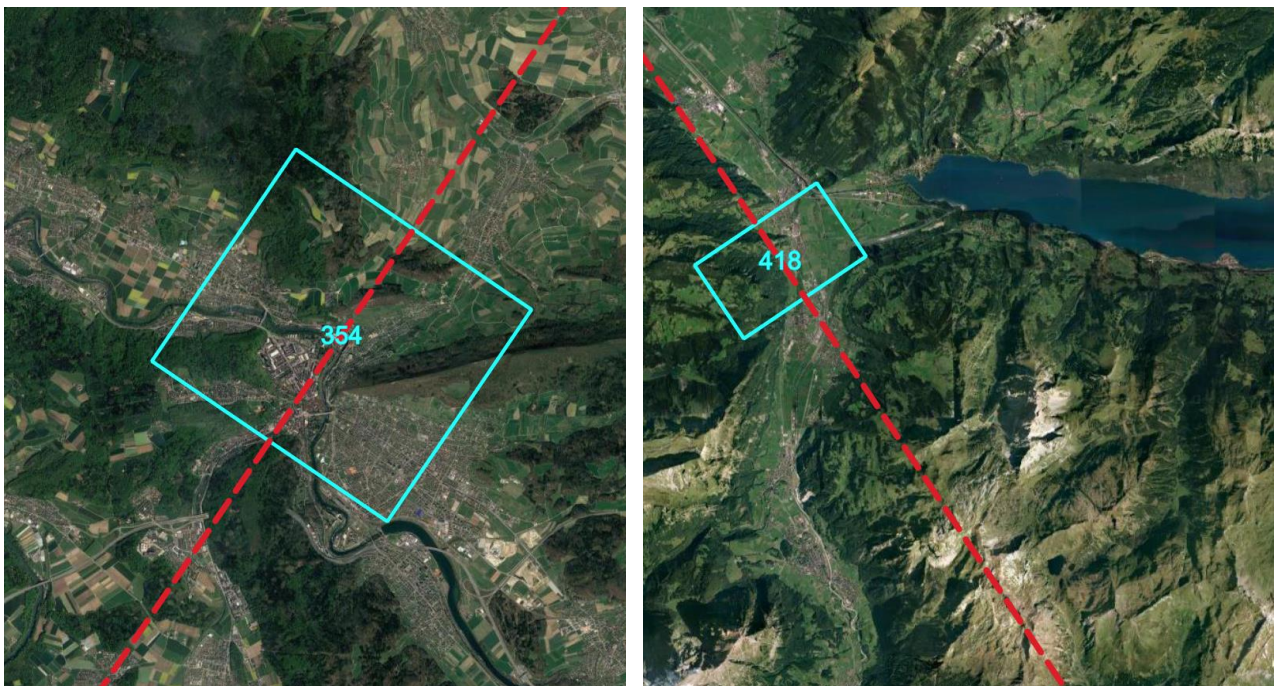
We also considered the database of virtual stations covering hydrological targets already used to generate the OLTC tables of Sentinel-3 A and B, Sentinel-6, and Jason-3. This database essentially consists of polygons, located over water



<b>ASSESSMENT OF CLOSED LOOP MODE PERFORMANCE AND FEASIBILITY OF AN OPEN LOOP MODE FOR SARIN MISSIONS</b>	Ref	NOV-FE-0747-NT-013		
	Issue	1	Date	21/03/23
	Rev	0	Date	21/03/23
	Page	12/36		

bodies overflowed by the corresponding satellites. Each entity has numerous attributes such as the type of hydrological target (lake, river, reservoir...), its reference elevation in meters, or the across-track distance in meters between the station and the targeted water body. As the elevations of the virtual stations are originally referenced to the Topex ellipsoid and the GGMO2C geoid, they were referenced to the WGS84/EGM96 system for this study. To do so, we subtracted the EGM96 geoid elevations, sampled under the ground tracks of each mission, from the corresponding GGMO2C elevations, which were all provided in the database. We then associated each virtual station center with its closest sampled ground-track point, and applied the computed geoid correction to the elevation. Finally, to do the ellipsoid conversion, as the height difference between the Topex and WGS84 ellipsoid is 70 cm at the equator, and 71.3682 cm at the poles, we simply subtracted 70 centimetres from every virtual station elevation. Given that we will not examine biases at centimetre level, this approximation should not have any consequences on the results.

In this analysis, we will only use virtual stations with an across-track distance attribute equal to zero (water bodies located at nadir), see Figure 3.



**Figure 3: Two examples of virtual stations, with the reference elevation displayed in meters. Those virtual stations were generated for the Jason-3 mission. On the left, the distance attribute is equal to zero, and the virtual station is indeed located on the river. On the right, the virtual station is located 3938 meters away from the lake beside it. The red dashes represent the Jason-3 ground track.**

Ref	NOV-FE-0747-NT-013		
Issue	1	Date	21/03/23
Rev	0	Date	21/03/23
Page	13/36		

## 2.4. Other datasets

We also used hydrological masks to select the CryoSat-2 POCA points located on water bodies such as lakes or rivers.

### 2.4.1. HydroLakes database for lakes

For lakes, we used the HydroLakes database [RD8]. It is a digital map created by compiling, correcting and unifying many near-global and regional datasets, including all lakes with a surface area exceeding 10 ha, at a global scale. This database stores lake contours as polygons (see Figure 4). We will consider the POCA points located within these contours.

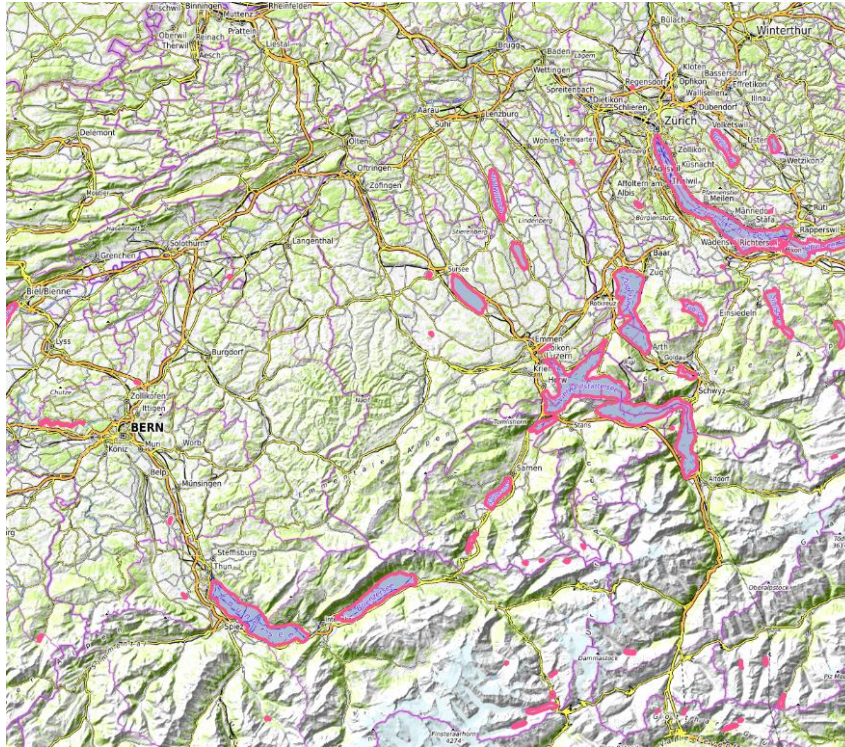


Figure 4: Visualisation of the Hydrolakes database, focused on the North of Switzerland. We can notably see Lake Zug, Lake Sempach and Lake Lucerne.

### 2.4.2. River contours

Furthermore, we selected POCA points located on rivers by crafting our own river mask, combining multiple sources. First, we retrieved data from the Global Surface Water Explorer (Joint Research Centre, JRC. Database and documentation are found in [RD9] and [RD10]). This dataset is a global surface water mapping with a 30-meter spatial resolution. Each pixel gives the occurrence of the presence of water during the 1984-2020 period (37 years), as a percentage ranking from 0% for a total absence of water to 100% for a permanent presence of water. We applied a threshold of 30% on the data in order to account for the seasonality of the width of some rivers. The pixels with a water presence occurrence higher than 30% form a first water mask. This first water mask is very good for large streams but not so much for smaller ones (see Figure 5).



Ref	NOV-FE-0747-NT-013		
Issue	1	Date	21/03/23
Rev	0	Date	21/03/23
Page	14/36		

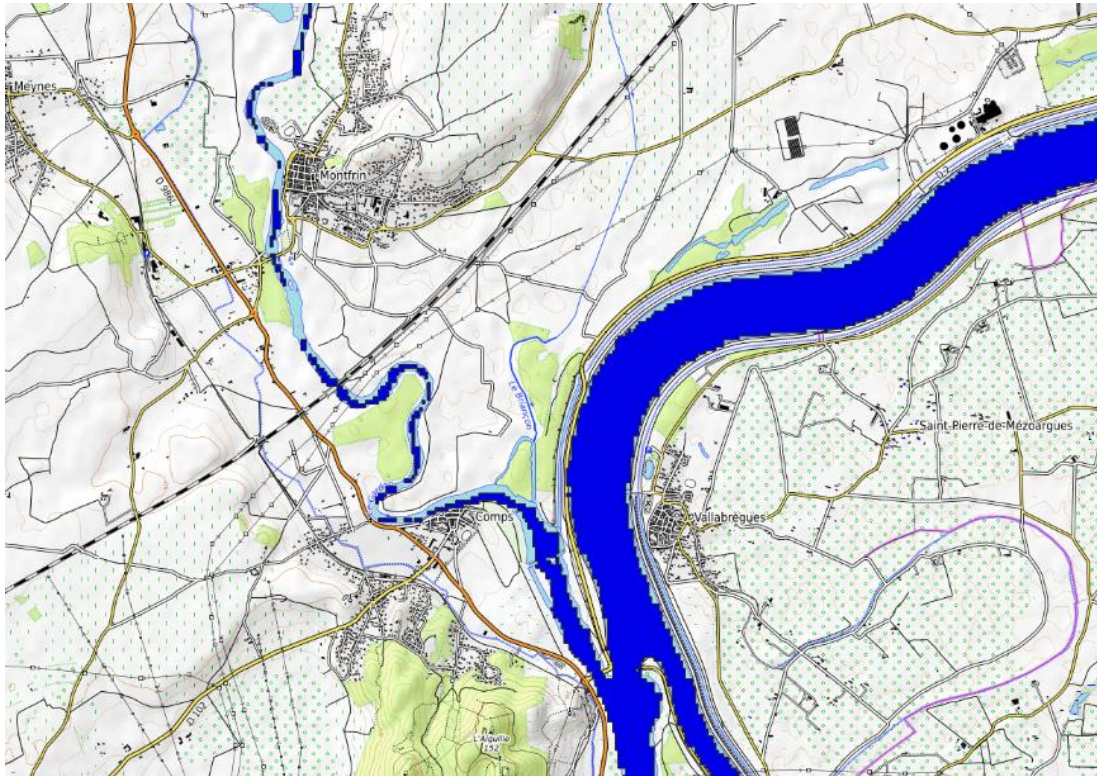


Figure 5: Example of the JRC mask (in blue) on the Rhône. We can see that its tributary on the left, the Gardon, is only partially accounted for.

To build a more precise mask and complete the JRC water mask, we merged it with the EU-Hydro River Network Database, from the Copernicus Land Monitoring Service (Database and documentation are found in [RD11] and [RD12]). This geodatabase contains lines describing all the European basins with a high level of detail. Two treatments had to be done to this dataset. First, the available level of detail was too high (see Figure 6). Therefore we filtered the data to only keep the main rivers. Each stream in the database was provided with its Strahler number, i.e. its position in the ramification of the river network. A stream with a Strahler number of 1 has no tributary whereas a powerful river like the Rhône is of order 8. We thus filtered out the streams with a Strahler number lower than 4, empirically chosen threshold. The comparison before and after the filtering is shown in Figure 6. Then, the data are distributed as lines and we needed polygons to perform intersections with CryoSat-2 POCA points. We simply applied a buffer on the remaining lines, giving them a width of about 300 meters (the width has been deliberately exaggerated to maximize the number of points selected near the rivers). The last step is to merge this new geometric data with the previous JRC mask.

We applied this process on the Rhône, Po and Danube basins, which gave the final mask visible on Figure 7.



Ref	NOV-FE-0747-NT-013		
Issue	1	Date	21/03/23
Rev	0	Date	21/03/23
Page	15/36		

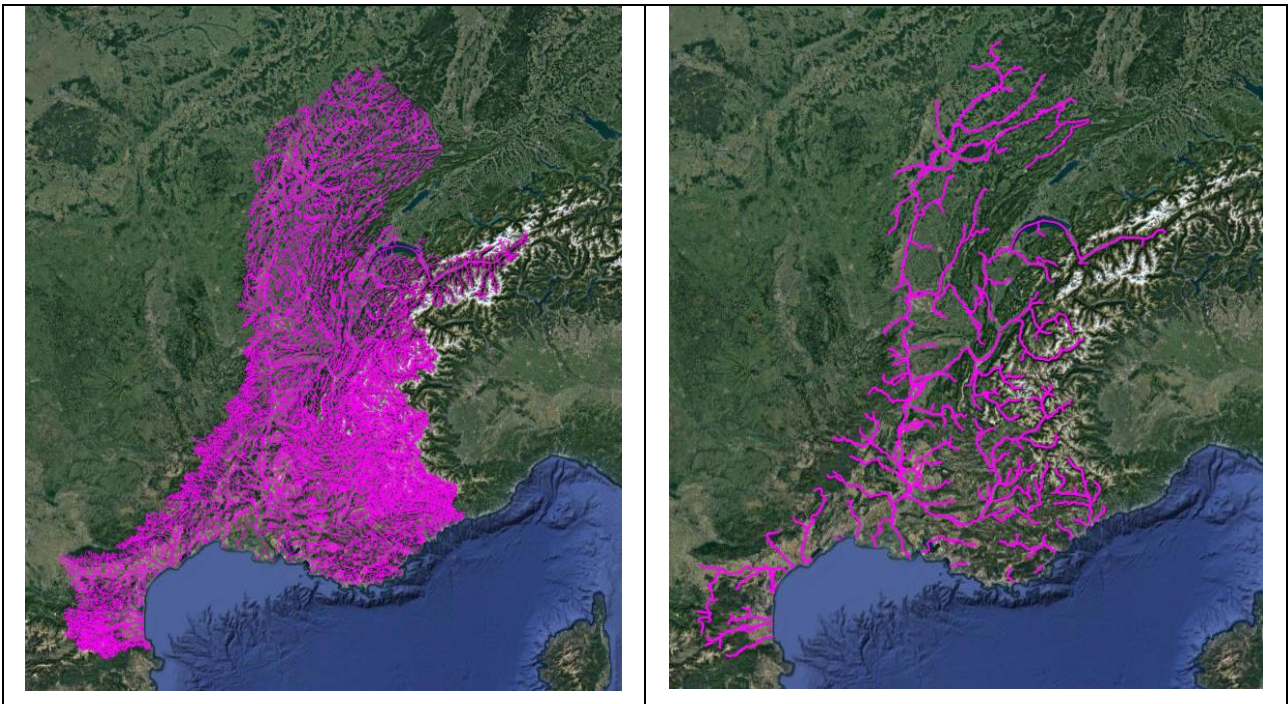


Figure 6: Visualization of the EU-Hydro Database over the Rhône basin. On the left, the database is shown without any filtering. On the right, only the streams with a Strahler number  $\geq 4$  are shown.



Figure 7: Final river mask combining the Rhône, Po and Danube basins.

### 3. General diagnostics on the zone of interest

#### 3.1. Data quality

The first step of our analysis was to check for flagged data, in order to filter the CryoSat-2 measurements and to keep only supposedly accurate heights. For heights, we used the “height\_1\_20\_ku” parameter. At level 2, Cryosat uses various retracking algorithms, leading to potentially multiple different height measurements for the same mode: height\_1, height\_2, height\_3 and so on. However, in SARin mode, only one algorithm, derived from the Wingham/Wallis model fit, is used. Therefore, the only height variable we considered was *height\_1\_20\_ku*.

Then, we assessed the quality of the data. The L2 CryoSat-2 products provide a quality flag (*flag\_quality\_20\_ku*), which indicates whether any of the measured values are erroneous. This binary flag is coded on 12 bits. Each bit corresponds to a specific error. When a specific error occurs, the bit value is set at 1. The final value is rendered in a decimal base. For instance, 4096 corresponds to an error on the “height\_1” value, and 32 corresponds to an error on the echo shape. Therefore a point with a quality flag value of 4128 has an error on the height and echo shape measurements.

We compared the data quality of the measures acquired over the Alps and the Siberian lakes throughout the year 2019. As mentioned before, those two areas differ a lot in terms of height variability. The purpose of this first analysis is to assess whether the Alps represent a suitable worst-case zone to study the SARin limitations for detecting inland water bodies. We listed all the possible values for the quality flag for all the points of the dataset, and computed their proportions within each dataset. The results are shown in Figure 8 and Figure 9. First, on both datasets, **all points** simultaneously show errors on the across-track angle, the significant wave height (which is irrelevant as our measurements are collected over land) and the altimeter wind calculation. However, on the Siberian Lakes dataset, only an infinitesimal proportion of the points also show an error on the height, whereas the Alps dataset has 35% of its points flagged with height errors.

Possible errors on the dataset. Total number of points: 528357		
Errors	Nb of occurrences	Percentage
‘xtrack_angle_error’ + ‘alt_wind_error’ + ‘swh_error’	528118	99.96 %
‘height_1_error’ + ‘alt_wind_error’ + ‘swh_error’	117	0.02 %
‘height_1_error’ + ‘sig0_1_error’ + ‘alt_wind_error’ + ‘swh_error’	122	0.02 %

Figure 8: Errors flagged on the Siberian Lakes dataset. All the points in the dataset are flagged with one of the three error combinations shown in the table. There are no points without error.

Possible errors on the dataset. Total number of points: 310990		
Errors	Nb of occurrences	Percentage
‘xtrack_angle_error’ + ‘alt_wind_error’ + ‘swh_error’	202248	65.03 %
‘height_1_error’ + ‘alt_wind_error’ + ‘swh_error’	246	0.08 %
‘height_1_error’ + ‘sig0_1_error’ + ‘alt_wind_error’ + ‘swh_error’	108496	34.89 %

Figure 9: Errors flagged on the Alps dataset. All the points in the dataset are flagged with one of the three error combinations shown in the table. There are no points without error.



### 3.2. Biases

To go further, we sampled the height of the ACE2 reference DEM under each POCA point, and computed the difference between this reference and the measured height. We then compared the distribution and magnitude of the biases between both datasets, after filtering out the points flagged with height errors. The results are shown in Figure 10. In the Alps zone, even though the points with height errors have been filtered out, 22% of the points in the Alps still show a bias superior to 50 meters, whereas more than 98% of the points from the Siberian Lakes dataset show biases under 20 meters.

Figure 11 shows where the biggest biases are located in the Alps zone. It appears that the biases superior to 1000 m are located deeper into the mountain range than the biases superior to 500 m, while those superior to 200 m are concentrated in the periphery of the mountains. This suggests that the height variability still degrades the performance of the SARin instrument, even after filtering out flagged points.

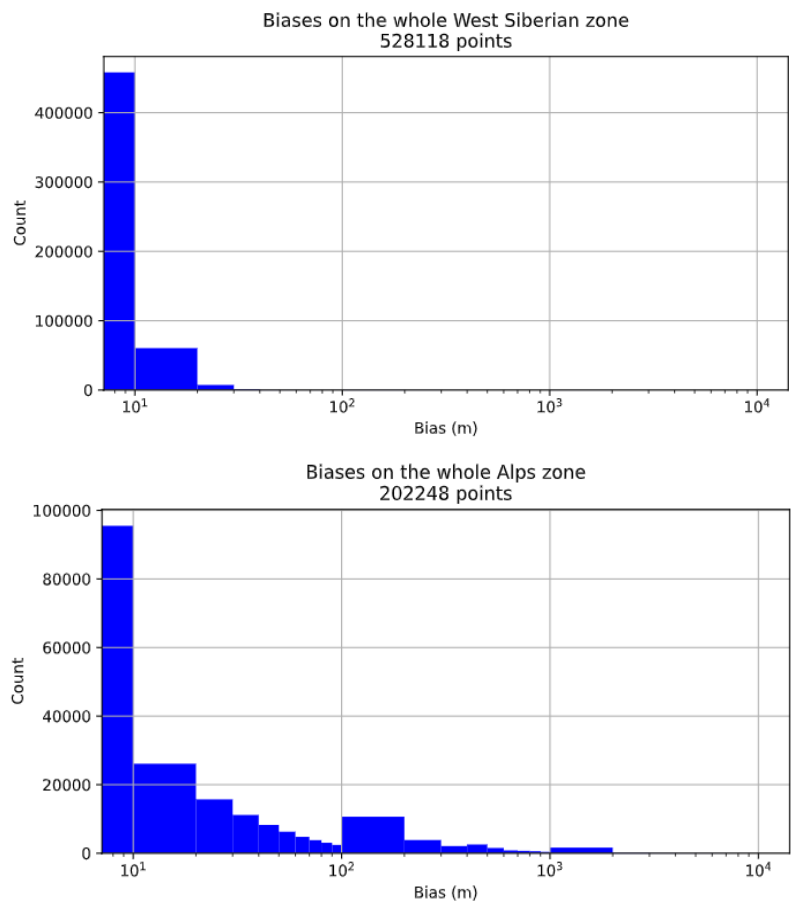


Figure 10: Biases on the West Siberian Lakes and Alps zones, with the ACE 2 DEM as reference.

Ref	NOV-FE-0747-NT-013		
Issue	1	Date	21/03/23
Rev	0	Date	21/03/23
Page	18/36		

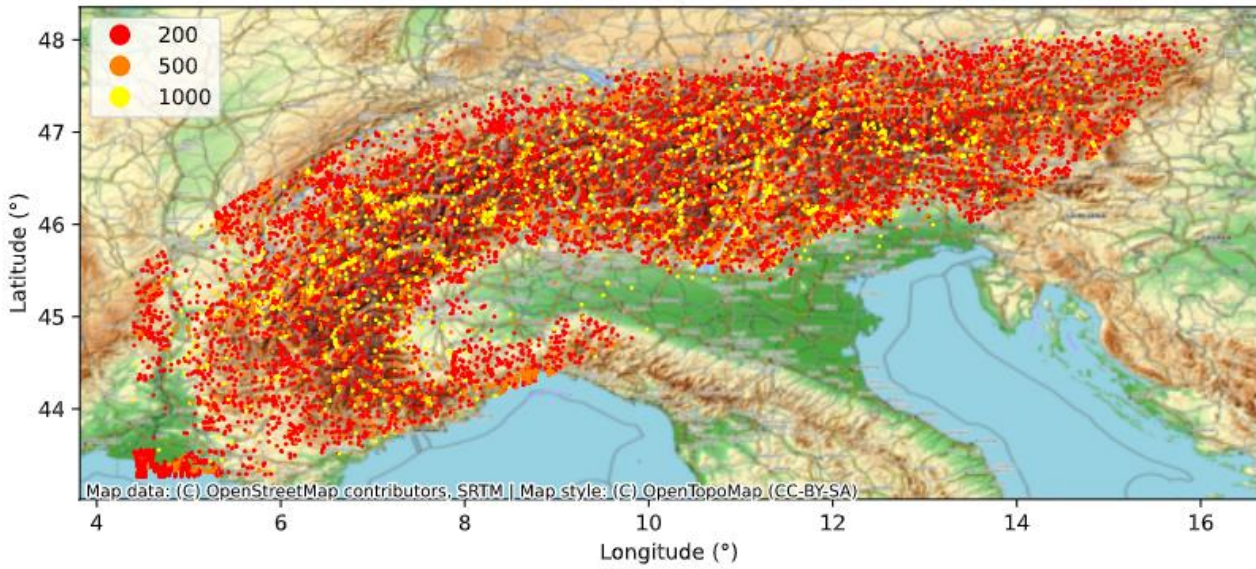


Figure 11: Visualisation of the strongest biases. Biases superior to 200 m are shown in red, to 500m in orange, and to 1000m in yellow.

We now repeat the same analysis, but this time we focus on hydrological targets. In order to select a suitable subset of the data, we have performed two intersections. First, we selected the POCA points located on the water mask described in section 0. We then intersected the selected points with the OLTC virtual stations. In the end the remaining points are located on water bodies, and contain information provided by the virtual station database (reference elevation, type of hydrological target...). We finally filtered out the points flagged with height errors. The remaining points and their biases are respectively shown in Figure 12 and Figure 13. We find the same pattern as before, with the largest biases located where the mountains are high, and the smaller ones in the periphery of the Alps.

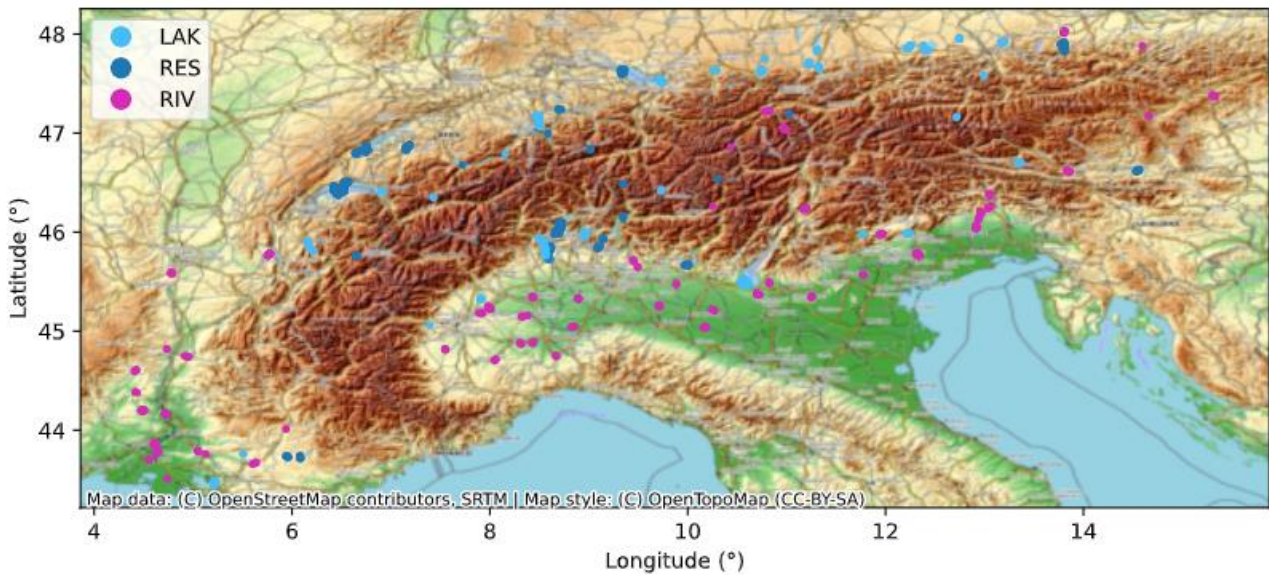


Figure 12: POCA located on hydrological target, coloured according to their type: LAK = lake, RES = reservoir, RIV = river.

Ref	NOV-FE-0747-NT-013		
Issue	1	Date	21/03/23
Rev	0	Date	21/03/23
Page	19/36		

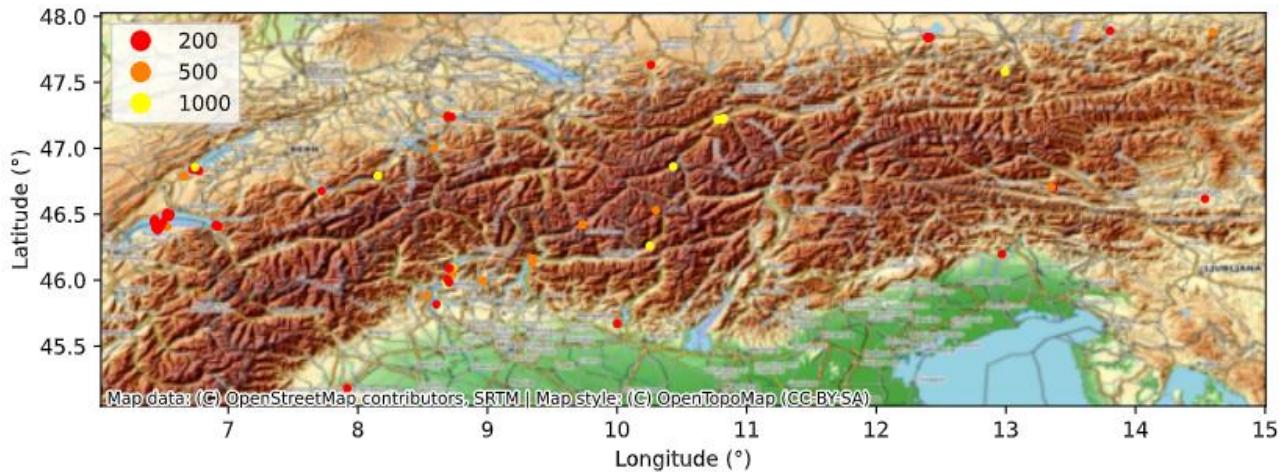
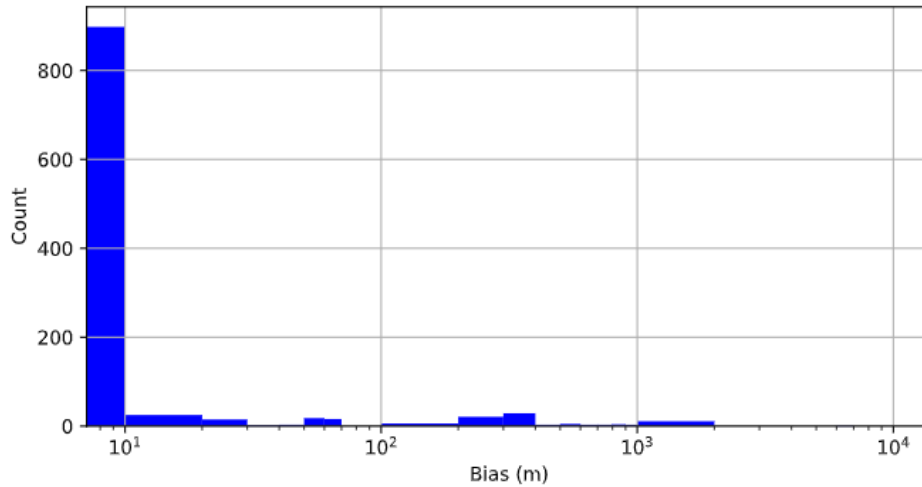


Figure 13: Biases of the POCA points located on hydrological targets, and locations of the largest biases.

We focused on a few points showing strong biases (superior to 200 m), and studied in which context those biases occur. Here are the most frequent cases encountered:

- A point showing a strong bias is an isolated unflagged point in a series of points flagged with height errors; see Figure 14a).
- A point showing a strong bias belongs to a series of points also showing important biases; see Figure 14b).
- A point showing a strong bias has a mix of the characteristics mentioned above, and belongs to a chaotic series rapidly alternating flagged points and unflagged points with large biases; see Figure 14c).
- A point showing a strong bias is isolated far beyond the theoretical swath of the SARin instrument; see Figure 14d).



Ref	NOV-FE-0747-NT-013		
Issue	1	Date	21/03/23
Rev	0	Date	21/03/23
Page	20/36		

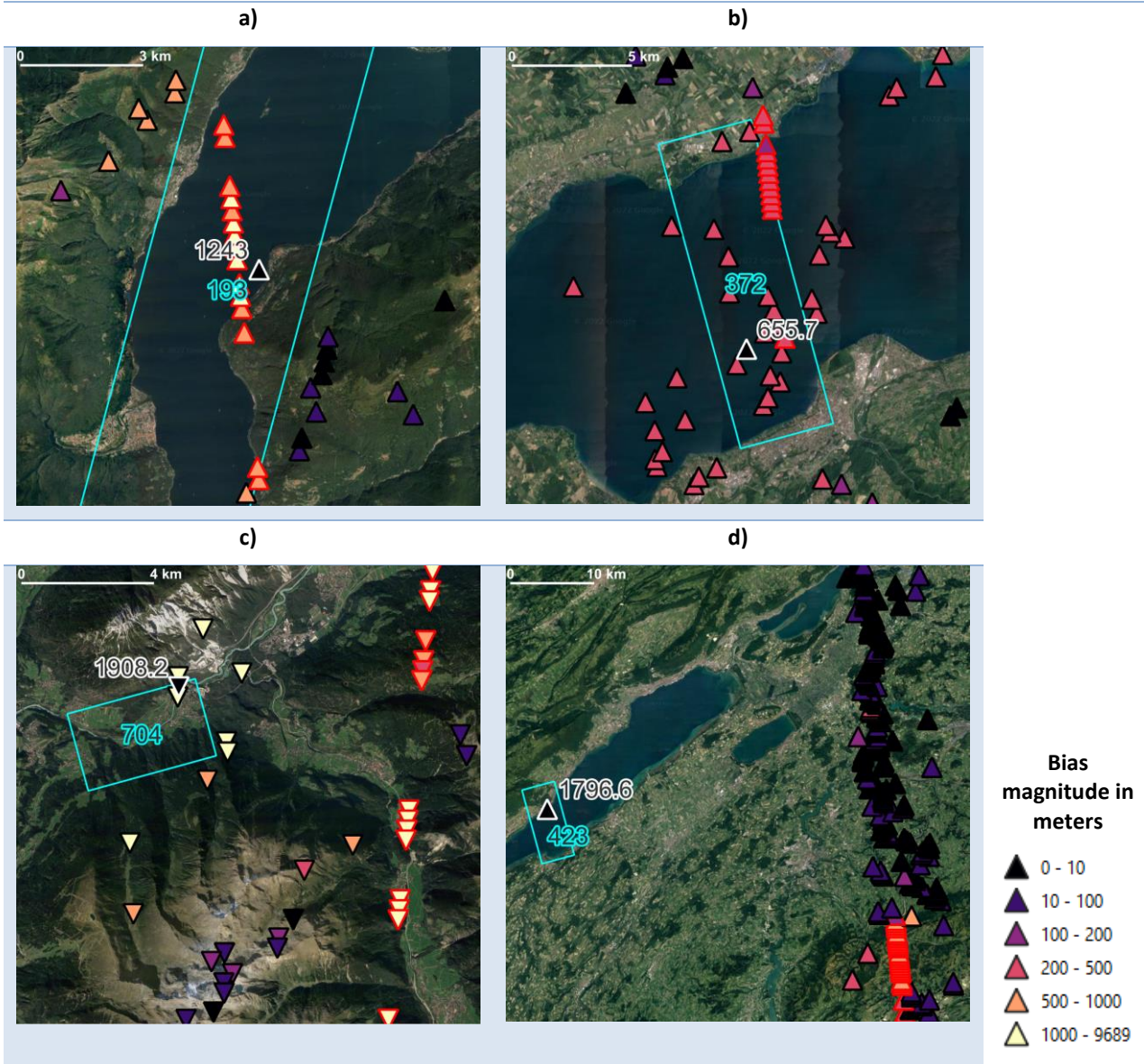


Figure 14: Examples of strong biases. The Cryosat points are shown as triangles oriented according to the satellite orbit direction. The point of interest in each image is the black and white triangle; its measured height is displayed in the same colours. The corresponding virtual station is displayed with its reference elevation in cyan. The other points form the corresponding Cryosat track, coloured according to the magnitude of the difference between their measured height and the associated ACE 2 elevation. The flagged points have red edges. The locations are: a) Lake Maggiore, Italy; b) Lake Geneva, Switzerland; c) Inn river, Austria; d) Lake Neuchatel, Switzerland.

At this point we also noticed that when a point is flagged with a height error, the POCA coordinates are by default set to the nadir coordinates.

Most of the large biases seem to come from incorrect measures, although they were not flagged as such by the retracking algorithm. At this stage, it is still difficult to identify the origin of these errors. However, as mentioned before, the magnitude and proportion of biases are much stronger in areas with high height variability. A particularly eloquent example of this phenomenon is visible on Figure 15, where only the ascending orbits of CryoSat-2 are shown on Lake Garda, Italy. When overflying the South of the lake, which is located in a relatively flat area, CryoSat-2 provides accurate height measurements in comparison to the ACE 2 reference, and almost none of the points are flagged. However, as the satellite goes northward and passes above the Alps, numerous points are flagged and biases start to rise. In this particular case, this suggests that the implementation of an a priori elevation to adjust the reception window of the



Ref	NOV-FE-0747-NT-013		
Issue	1	Date	21/03/23
Rev	0	Date	21/03/23
Page	21/36		

SARin instrument could reduce the number of errors and improve its performance. We also notice that the POCA points tend to follow the banks of the lakes.

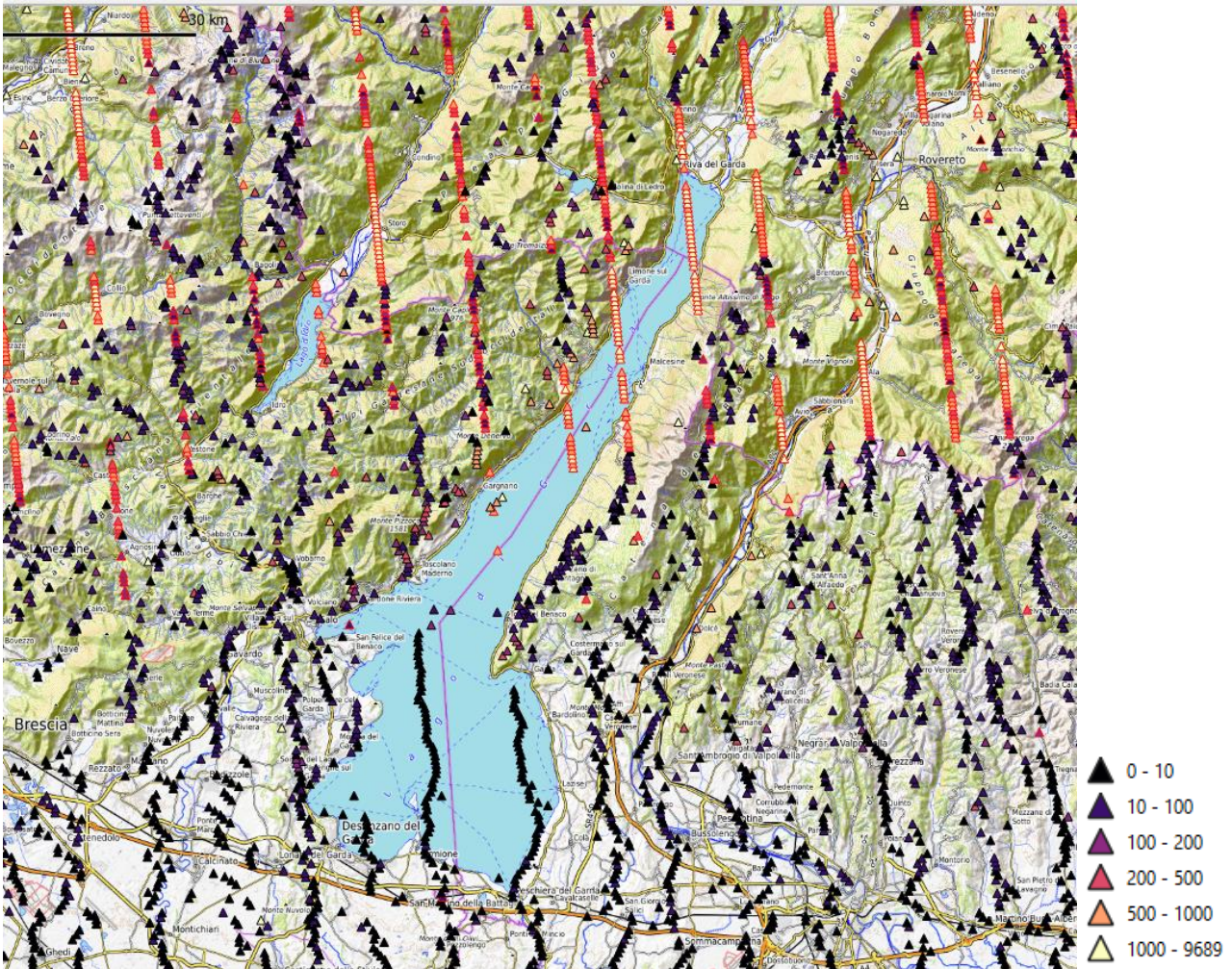


Figure 15: Topographic map of Lake Garda, Italy. The Cryosat points are represented with the same method as in Figure 14, displaying only ascending orbits.



Ref	NOV-FE-0747-NT-013		
Issue	1	Date	21/03/23
Rev	0	Date	21/03/23
Page	22/36		

## 4. Case study: Lake Geneva

In this section we will address the CryoSat-2 performances on a large hydrological target located in the Alps Mountain range: Lake Geneva. We selected this lake because it is one of the largest lakes in the Alps, and CryoSat-2 flies over it 22 times in a single cycle. This offers a significant volume of data to analyse. This lake also drew our attention because it provides many different cases that are worth studying in detail:

- Tracks that are mostly composed of accurate points.
- Tracks that are mostly composed of unflagged but dispersed points showing strong biases.
- Tracks mostly composed of flagged points, whereas the points located on land are unflagged and often accurate.

Examples of those cases are respectively shown from left to right in Figure 16. This section aims at investigating and identifying the origin of the observed errors, by looking at the SARin waveforms distributed in the CryoSat-2 L1B products. In addition to using data over the whole year 2019, we will also consider products from other years (i.e. other cycles, see §0), for a few selected orbits only, in order to examine the variation over time of the SARin performance on the same area.

The L1B products give the power waveform in a compressed format, in order for each waveform to fit into two bytes. To compute the actual power waveforms in Watts, we will use the scale factor provided along with the compressed waveform values.

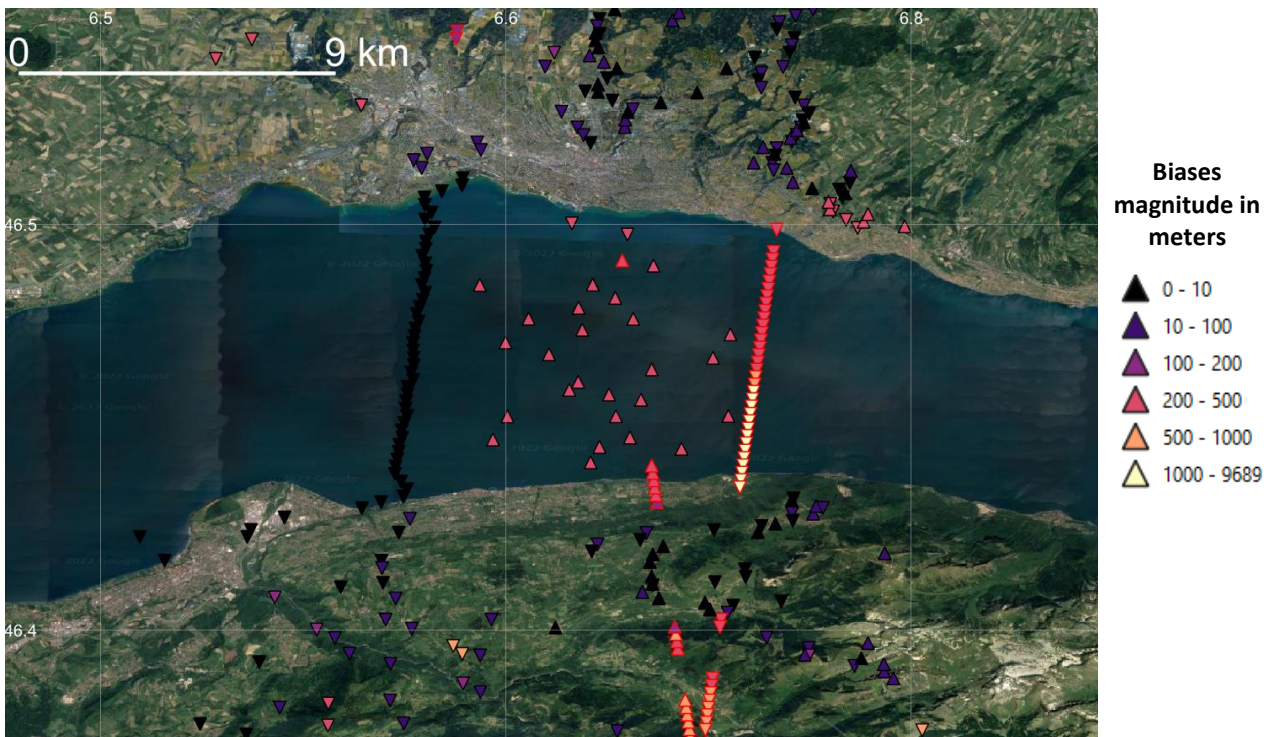


Figure 16: Three track examples on Lake Geneva. The absolute orbit numbers are respectively 46650, 50611 and 49112 from left to right. The Cryosat points are displayed with the same method as in Figure 14.

Ref	NOV-FE-0747-NT-013		
Issue	1	Date	21/03/23
Rev	0	Date	21/03/23
Page	23/36		

### 4.1. Comparing unflagged and flagged waveforms

In this section, we examine the waveforms of different types of point series over Lake Geneva, which are summarized above. Figure 17 displays the waveform corresponding to orbit n°46650 (January 26<sup>th</sup>2019). This is a particular case that seems correct from all points of view: the height measurements are in good agreement with the known heights of Geneva Lake, with a mean bias of no more than 10 centimeters over the lake; the waveform has a shape that allows an accurate retrieval of the altimeter height (good signal to noise ratio, high and well-centred peak); and the POCA points form a coherent and aligned series located on the lake.

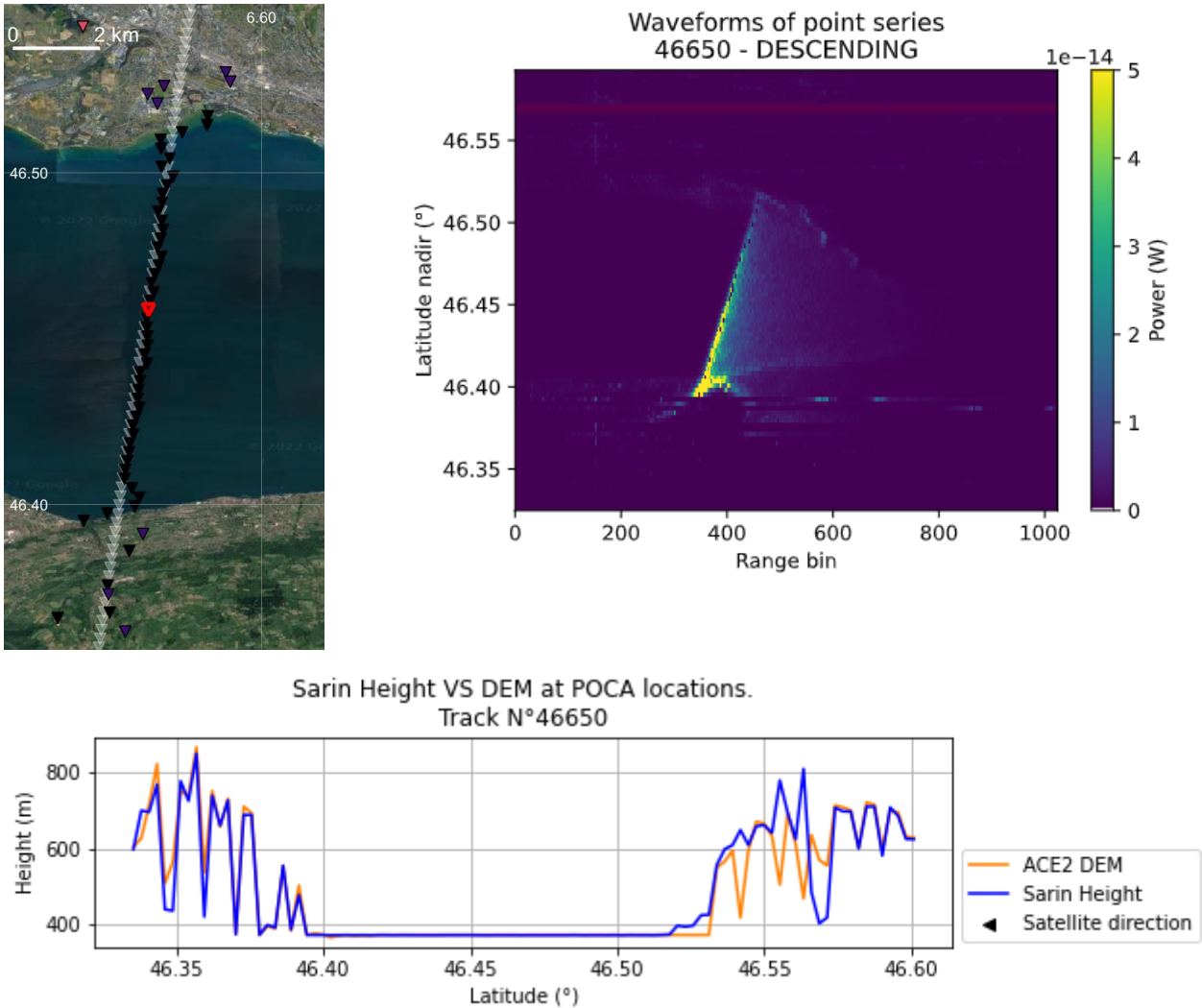
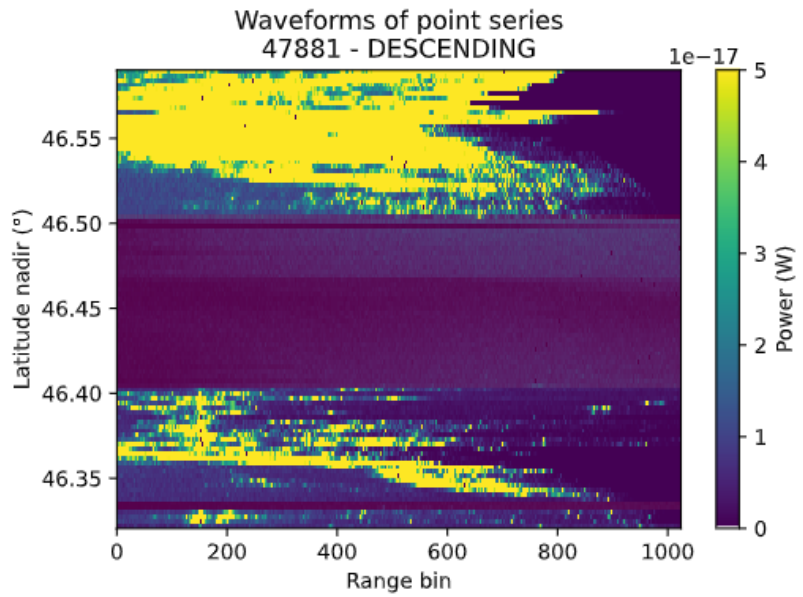
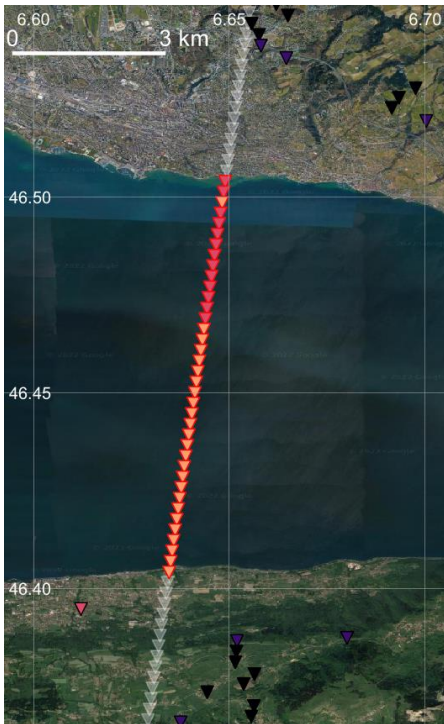


Figure 17: Power waveform for orbit n°46650 on Lake Geneva. The bottom plot gives a more detailed comparison of the altimeter height vs DEM height sampled under the POCA points. For visualization purposes, the reference coordinate is always the NADIR latitude of the point. The black triangle in the caption box indicates the satellite direction, i.e. ascending or descending.

We now look at a case where altimeter heights are all flagged with height errors. As mentioned in section 3.2, the flagged POCA points are located on the nadir coordinates, and show important biases. Oddly, in most cases this happens only over the lake, which is something that requires further investigation to be thoroughly understood. Figure 18 shows an example of this with orbit N°47881 (April 20<sup>th</sup>2019). The waveform has an extremely weak power on the lake area: around  $10^{-17}$  W, whereas the “clean” waveform in the previous case had a peak height around  $10^{-13}$  W. There is also no distinguishable peak; the waveform rather consists in a blurry patch of noise. Note that this is a different orbit than the one shown in Figure 16.

Ref	NOV-FE-0747-NT-013		
Issue	1	Date	21/03/23
Rev	0	Date	21/03/23
Page	24/36		



Sarin Height VS DEM at POCA locations.  
 Track N°47881

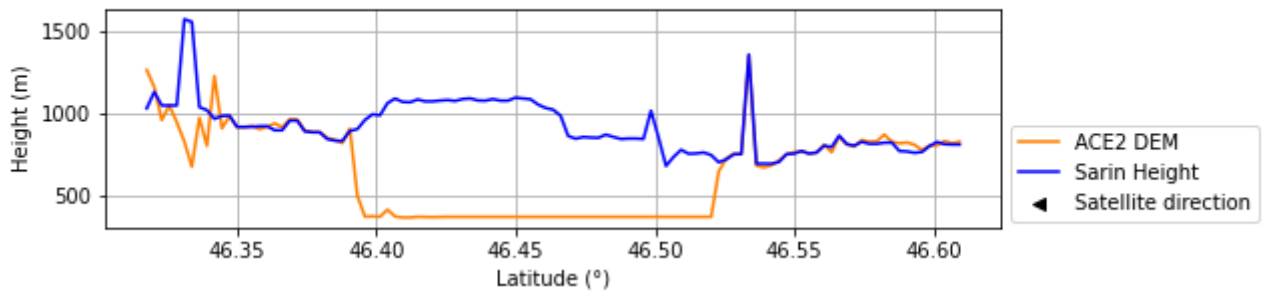
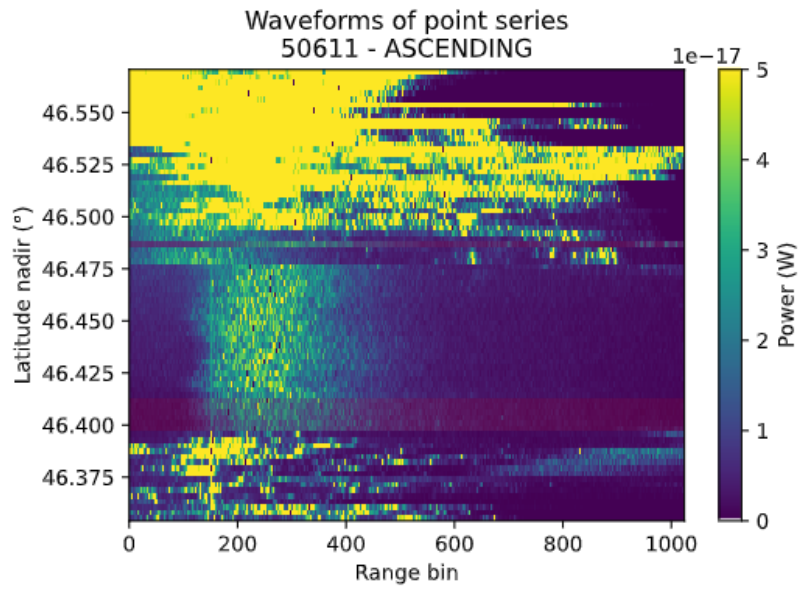


Figure 18: Power waveform for orbit n°47881 on Lake Geneva. On the waveform plot, the areas where the points are flagged are highlighted in red. The black triangle in the caption box indicates the satellite direction, i.e. ascending or descending.

Another case drew our attention: we found orbits with unflagged points, but with very scattered POCA coordinates, and showing important biases on the lake. Figure 19 shows such an example with orbit N°50611 (October 26<sup>th</sup> 2019). The waveform shows also a weak and noisy signal, located only on the lake area. However it seems that this signal is slightly stronger than on orbit N°47881, reaching powers around  $5 \times 10^{-17}$  W. It also appears that the noise peaks around bin N°250, as if it had the shape of a very smooth waveform like that seen in Figure 17. These characteristics might be responsible for the retracking algorithm not flagging those measurements, even though they do not allow an accurate computation of POCA height and position.



Ref	NOV-FE-0747-NT-013		
Issue	1	Date	21/03/23
Rev	0	Date	21/03/23
Page	25/36		



Sarin Height VS DEM at POCA locations.  
 Track N°50611

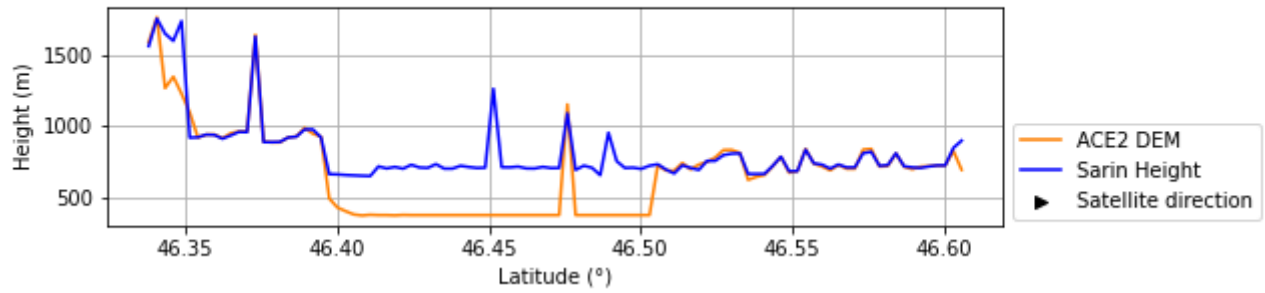


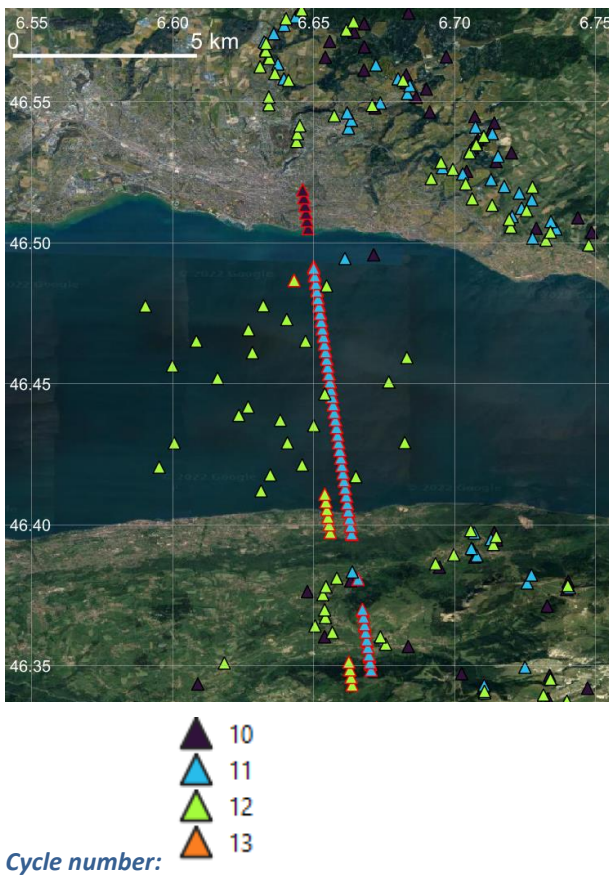
Figure 19: Power waveform for orbit n°50611 on Lake Geneva.

## 4.2. Comparing measurements over successive cycles

Until now, we have only studied measurements belonging to the 12<sup>th</sup> cycle of Cryosat. In order to see the consistency of the data accuracy over time, we also examine waveforms on areas overflown many times by the satellite. We take two reference orbits that we have already studied: orbit N°50611, which yielded the ambiguous results of scattered unflagged POCA points with wrong heights measurements (see Figure 19); and orbit N°46650, which yielded accurate measurements (see Figure 17). The respective relative – to the cycle - numbers of these 2 reference orbits are 4128 and 167.

### 4.2.1. Relative orbit number 4128

Figure 20 shows the selected orbits belonging to relative orbit N°4128, with the absolute orbit numbers and the corresponding dates of measurement. It already appears that, while most of the points from orbit N°50611 are unflagged, orbits N°45267 and 39923 have flagged points on almost the entire lake area.



Absolute orbit number                      Date




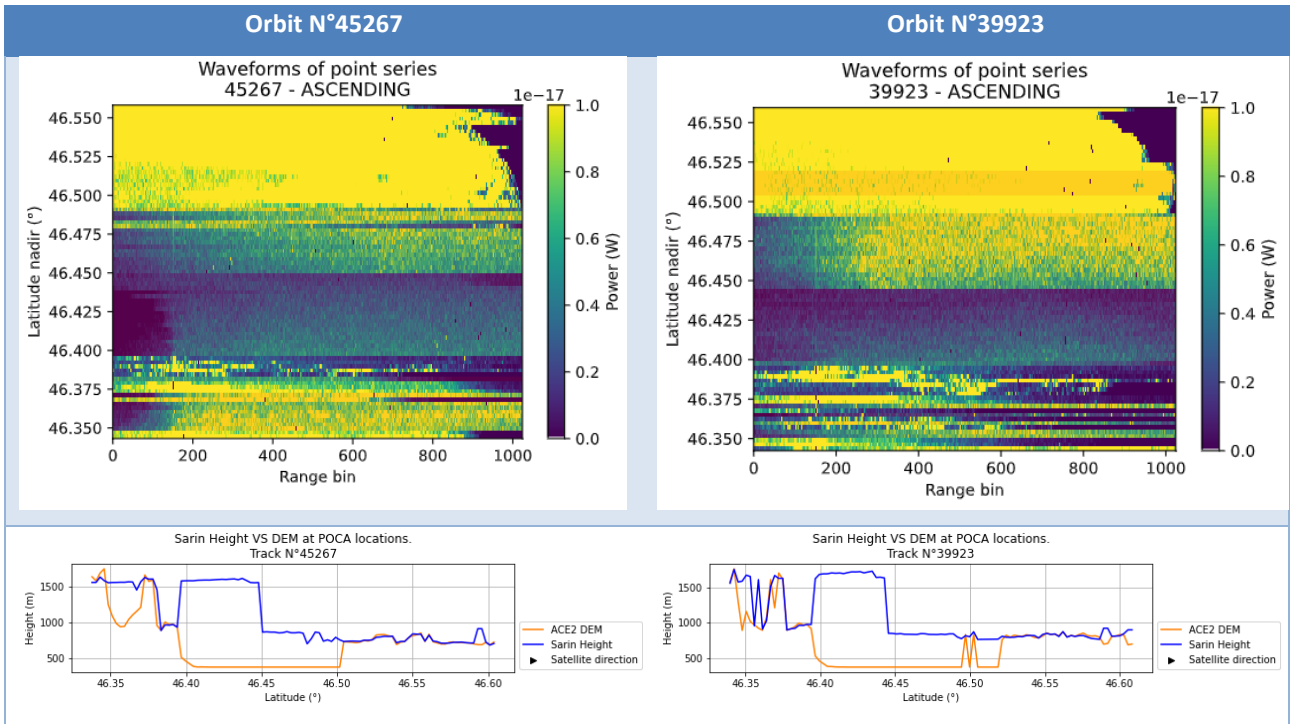
50611	2019/10/26
	
45267	2018/10/22
	
39923	2017/10/19
	

Figure 20: Selected orbits with relative orbit number equal to 4128. The POCA points are coloured according to their respective cycle numbers. Flagged points have red edges. Orbit N°39923 is barely visible because it is extremely close to orbit N°45267 and therefore masked by it at this zoom level.

When looking at the waveforms of orbits N°45267 and 39923, the same pattern as that previously observed with the entirely flagged orbit appears. There is a weak and noisy signal, as shown in Figure 21. There are also two very distinct altimeter height levels on the lake areas for both new orbits, with a visible and brutal transition around latitude 46.45°N.

Ref	NOV-FE-0747-NT-013		
Issue	1	Date	21/03/23
Rev	0	Date	21/03/23
Page	27/36		



**Figure 21: Waveforms and biases for orbits N°45267 and 39923**

#### 4.2.2. Relative orbit number 167

Figure 22 shows the selected orbits belonging to relative orbit N°167, with the absolute orbit numbers and the corresponding dates of measurement. Contrary to orbit 46650, which yielded accurate height measurements, the two other orbits mostly show flagged points over the lake. The details of the waveforms and biases are shown in Figure 23. Surprisingly, even though the points are flagged, the waveform is not noisy compared to the usual flagged ones. Its shape is actually very similar to that of orbit N°46650, with a clearly distinguishable peak and trailing edge. However, the signal is much weaker. While orbits N°51994 and 41306 show a peak in the order of  $10^{-14}$  W, orbit N°46650 shows a peak in the order of  $10^{-13}$  W. The two waveforms are also strongly shifted in the reception window. Regarding the measured heights, a noticeable bias (around 50 meters) appears on the lake.

Ref	NOV-FE-0747-NT-013		
Issue	1	Date	21/03/23
Rev	0	Date	21/03/23
Page	28/36		



-  10
-  11
-  12
-  13

Cycle number:

Absolute orbit number                      Date




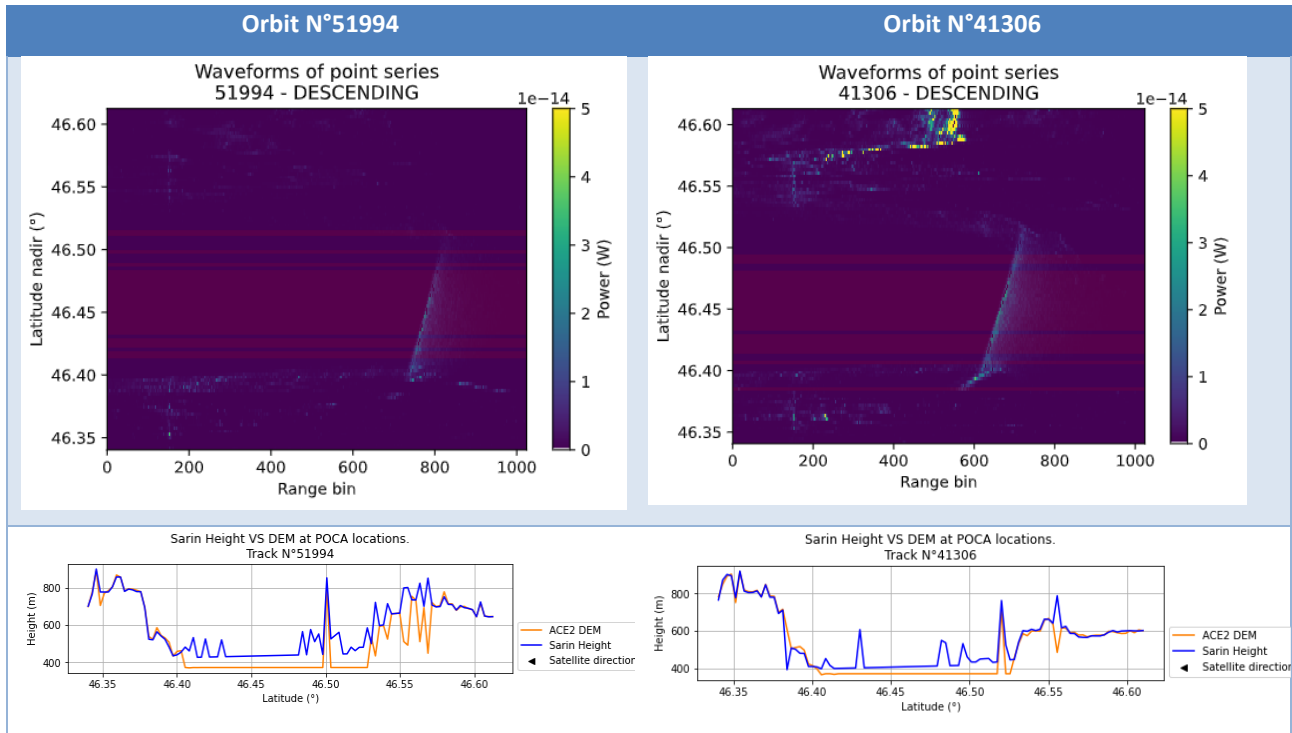
51994 	2020/01/29
46650 	2018/01/22
41306 	2017/10/19

Figure 22: Selected orbits with relative orbit number equal to 167. The POCA points are coloured according to their respective cycle numbers. Flagged points have red edges.

Ref	NOV-FE-0747-NT-013		
Issue	1	Date	21/03/23
Rev	0	Date	21/03/23
Page	29/36		



**Figure 23: Waveforms and biases for orbits N°51994 and 41306**

This case study over Lake Geneva showed that waveforms often abruptly become noisy and scattered when the SARin instrument flies over the lake. The altimeter seems to lose track as soon as it encounters the lake surface, whereas it detects objects on land. Our hypothesis is that before overflying the lake, the POCA points are not located near the nadir, but rather on the nearby mountain flanks. Therefore, when the water body becomes dominant under the altimeter, the POCA should suddenly be located several hundred meters under their previous positions, whereas the closed-loop tracking mode of the altimeter requires a much smoother elevation transition to properly center the reception window. This could be the reason why the altimeter was not able to retrieve data on the lake, and the data should be acquired again once the altimeter reaches the opposite bank. This would also infer that while Lake Geneva is one of the largest water bodies in Europe, it is still too incised in the mountains to allow reliable water surface level measurements with the SARin working in closed loop mode.

To support this hypothesis, we show in Figure 24 the status of many CryoSat-2 measurement points over Lake Victoria in Africa. The lake is surrounded by relatively smooth terrain, contrary to Lake Geneva. The ground track of CryoSat-2 is very dense, so only 1 out of 5 orbits are shown in Figure 24 a), for better readability. As seen on the figure, only a marginal fraction of POCAs is flagged with height errors, and it seems to happen only in areas where the topography becomes a little more heterogenous. The elevation profile in Figure 24 c) shows that the SARin measurements are in line with the ACE2 DEM, with an elevation range much smaller than Lake Geneva (less than 100 meters against several hundred meters). We notice two measurements that seem wrong: one at latitude  $\sim -2.47^\circ$ , flagged with a height error, and another at latitude  $\sim -2.12^\circ$ , not flagged. There is also a small gap near the shore of the lake at latitude  $\sim -2.15^\circ$ , which can be explained by the coarser delimitation of water bodies in the ACE2 DEM, mentioned in Section 2.3.



Ref	NOV-FE-0747-NT-013		
Issue	1	Date	21/03/23
Rev	0	Date	21/03/23
Page	30/36		

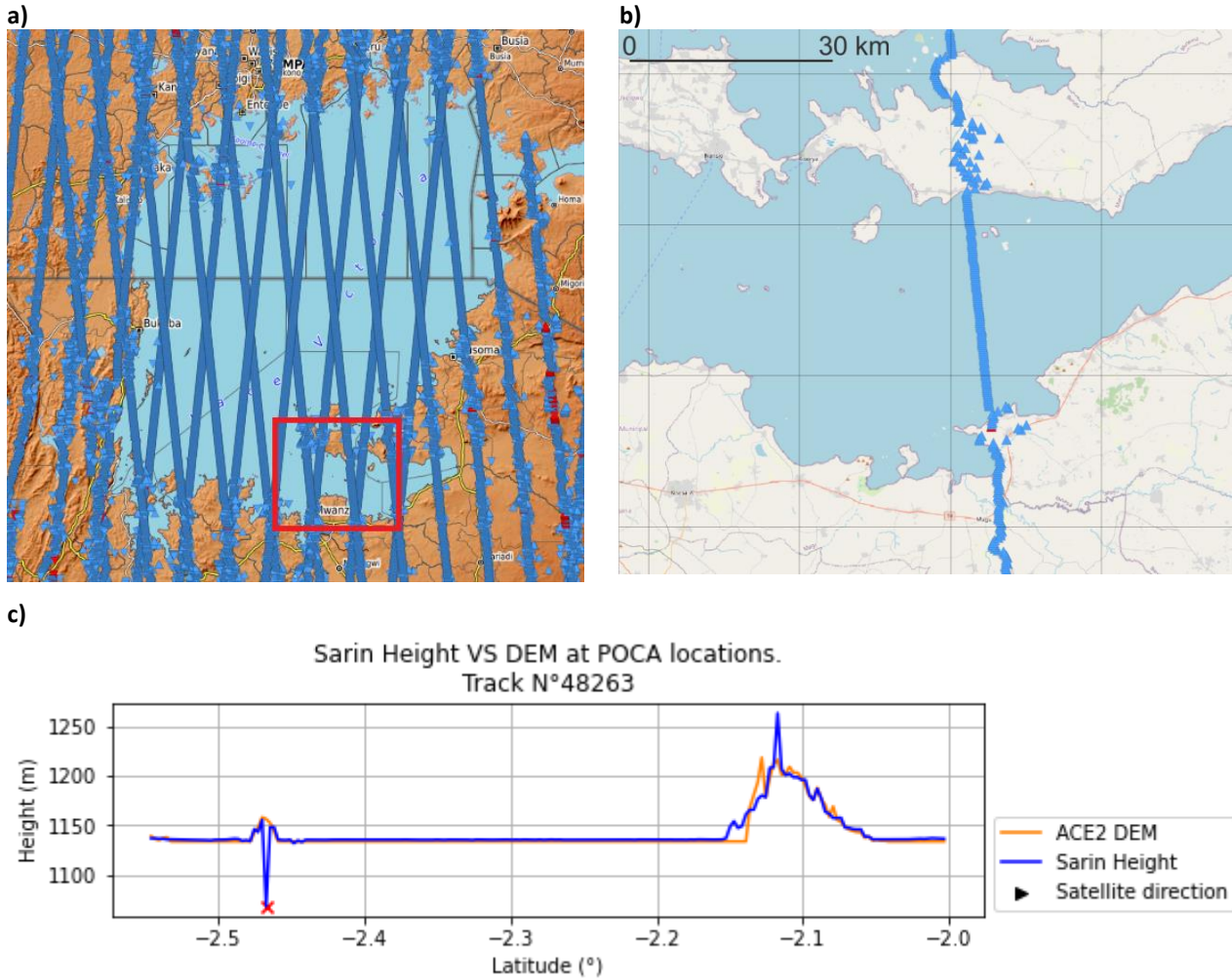


Figure 24: a) Overview of the POCA points over Lake Victoria. The POCA points are represented by triangles oriented according to the satellite direction. The points flagged with height errors are coloured in red, and the others in blue. The red square shows the area where we focus on orbit N°48263, isolated in b). c) shows its measured elevation profile, compared to the ACE 2 DEM, sampled under the POCA points. The POCA points flagged with height errors are shown by a red cross on the plot.

The heterogeneous nature of the terrain of mountainous areas is the key factor of the degradation of the CryoSat-2 SARin measurements over lakes. Therefore, it is safe to assume that defining an a priori elevation to center the altimeter's reception window would certainly improve the quality of the water height acquisitions.

Ref	NOV-FE-0747-NT-013		
Issue	1	Date	21/03/23
Rev	0	Date	21/03/23
Page	31/36		

## 5. Detecting rivers in mountainous areas

Other types of targets that are often difficult to detect with traditional space altimetry are rivers in mountainous areas. Such water bodies, embedded between two mountain sides, often go unnoticed by altimeters, as the steep slopes do not allow a proper autonomous adjustment of the centering of their reception windows. In this section we examine in detail, using a few examples, the performance of the SARin instrument in this respect. The points are selected using the water mask described in section 0, and we will use the Virtual Station dataset as reference for height. All points, whether they are flagged or not, are considered. Figure 25 shows that in the mountains, most of the remaining points are flagged with height errors.

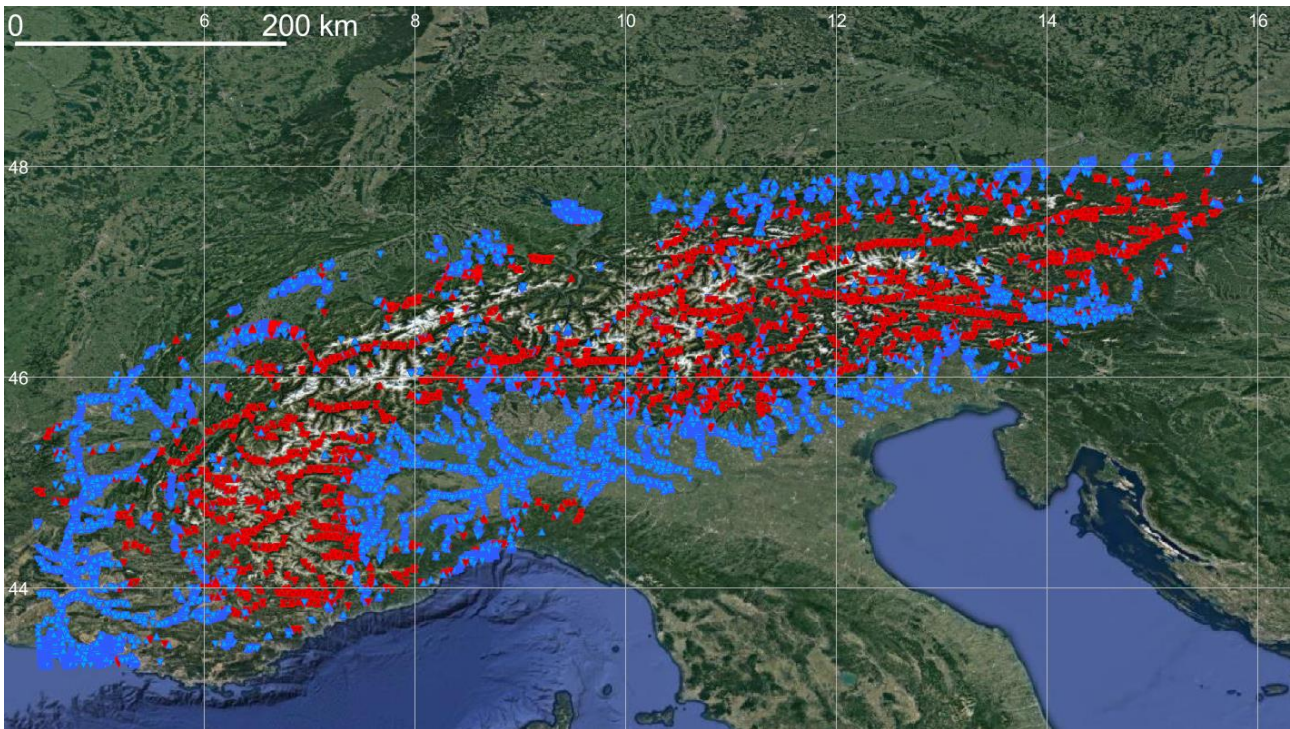


Figure 25: POCA points from 2019 after intersection with the water mask. Red points are flagged with a height error.

Figure 26 shows an example where the height measurements are accurate. On orbit N°447316, the POCAs are not flagged, follow the river and give consistent height measurements.



Ref	NOV-FE-0747-NT-013		
Issue	1	Date	21/03/23
Rev	0	Date	21/03/23
Page	32/36		

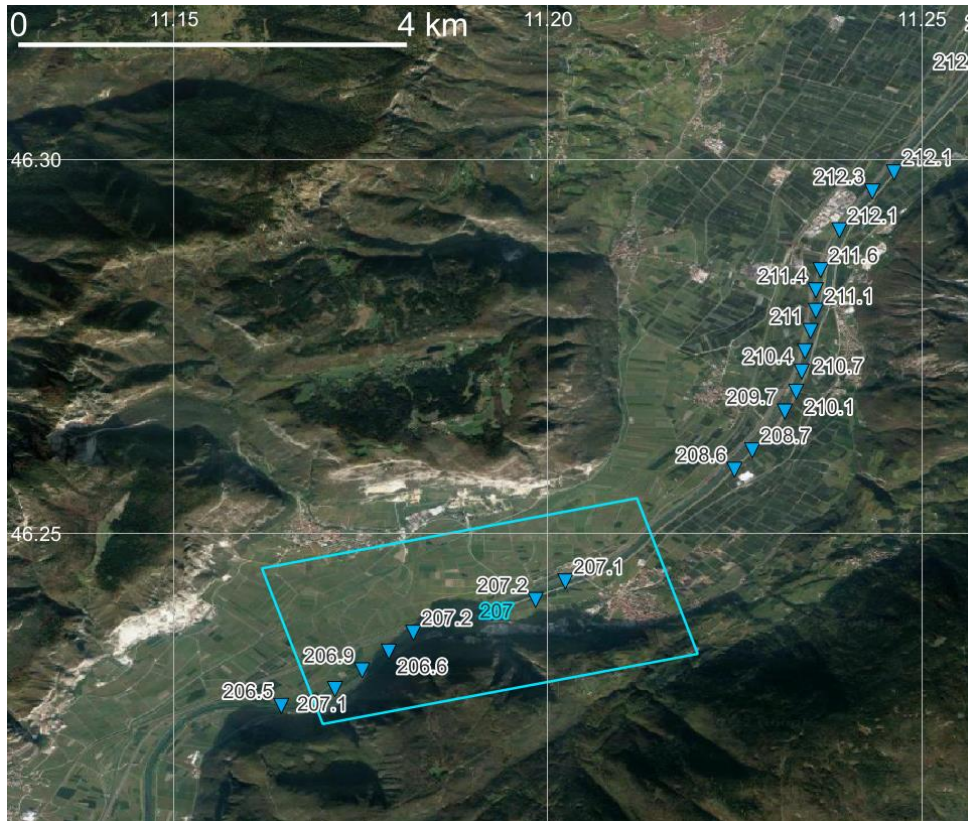


Figure 26: Focusing on orbit N°47316, intersecting with the Adige river, Italy.

However, this example is rather an isolated case. Most of the time, we are confronted with cases analogous to what is shown in Figure 27. It represents the intersection of many orbits (from left to right: 48605, 49386, 50104, 51067, 51335) with the Adda river in Italy. All those intersection points are flagged and obviously show highly inaccurate measurements. Looking into the waveforms in the L1B products (see Figure 28), it appears that the SARin loses track when flying over the valley where the river lies. Indeed, the five waveforms show a large patch of weak and noisy signal at these latitudes. It suggests that the altimeter does not have a well-centered reception window in this area. In that case the implementation of the OLTC on CryoSat-2 should be beneficial.



<b>ASSESSMENT OF CLOSED LOOP MODE          PERFORMANCE AND FEASIBILITY OF AN OPEN          LOOP MODE FOR SARIN MISSIONS</b>	Ref	NOV-FE-0747-NT-013		
	Issue	1	Date	21/03/23
	Rev	0	Date	21/03/23
	Page	33/36		

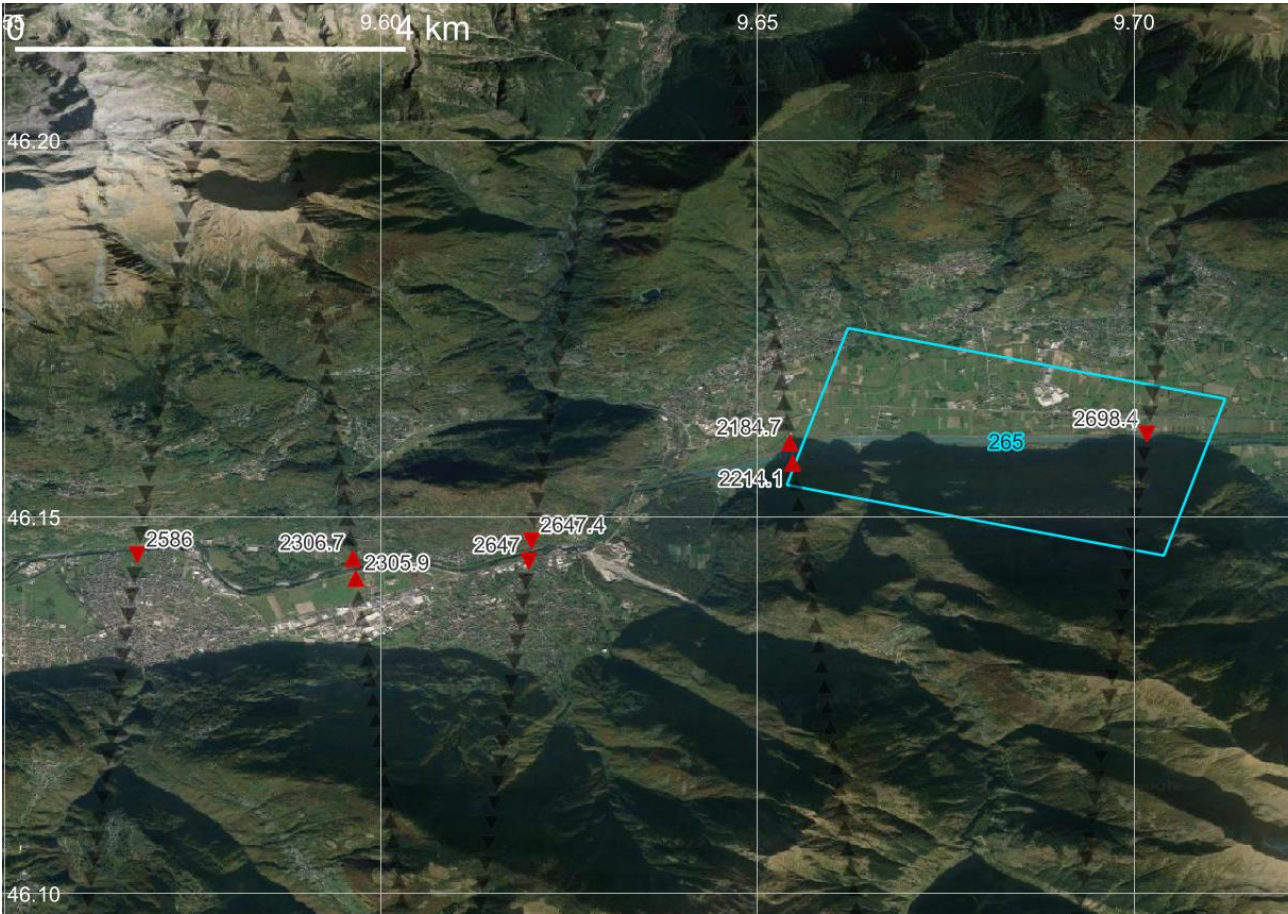
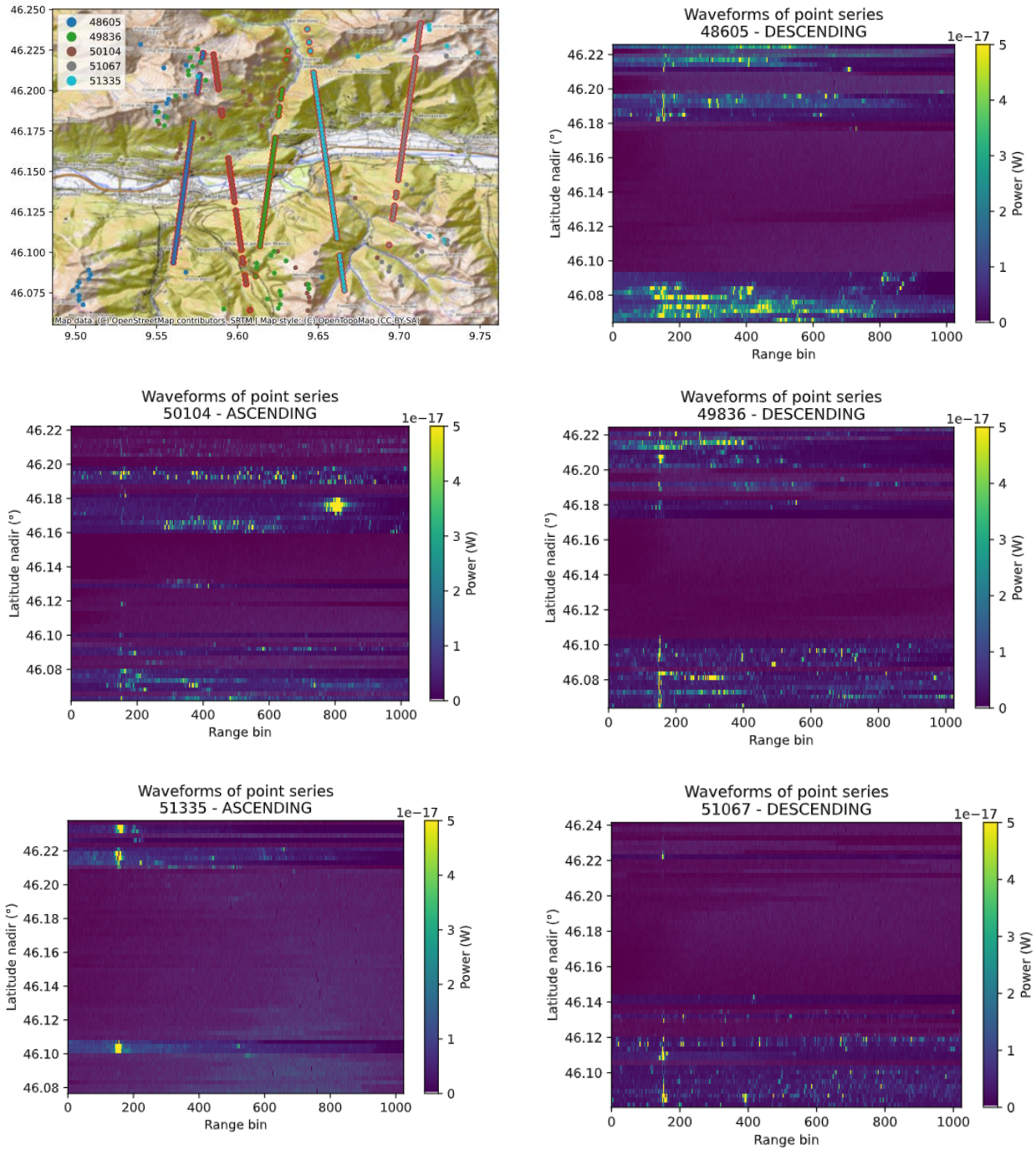


Figure 27: Intersection of many orbits with the Adda river, Italy. The cyan rectangle represents the local virtual station. The orbit numbers are respectively, from left to right: 48605, 49386, 50104, 51067, 51335.

Ref	NOV-FE-0747-NT-013		
Issue	1	Date	21/03/23
Rev	0	Date	21/03/23
Page	34/36		



**Figure 28: Waveforms over the Adda river**

This area is a typical case where an a priori elevation would be needed, so the altimeter does not lose track over the valley. As a comparison, the waveform obtained from the Sentinel-3 B nadir altimeter over the local virtual station is shown in Figure 29. The leading edge is clearly distinguishable.

Ref	NOV-FE-0747-NT-013		
Issue	1	Date	21/03/23
Rev	0	Date	21/03/23
Page	35/36		

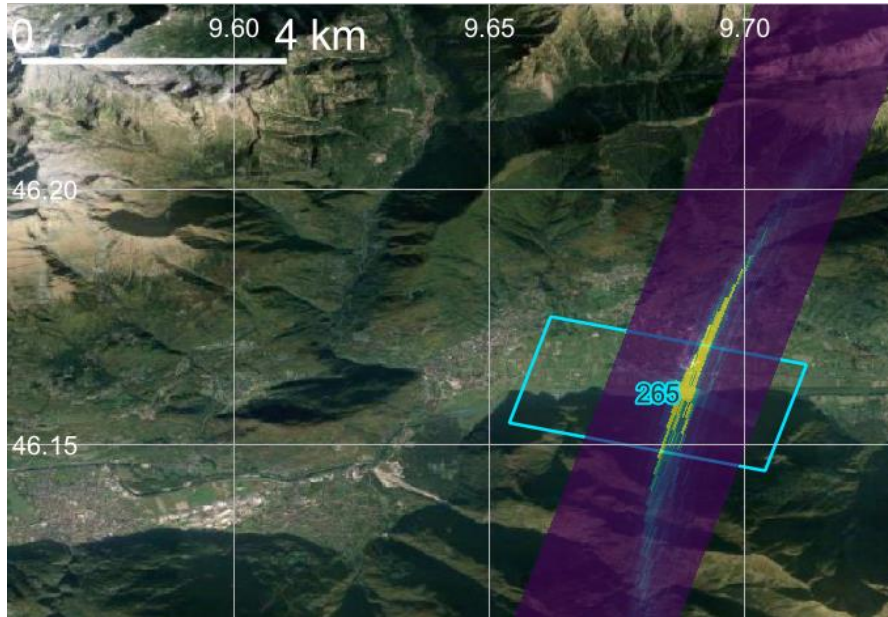


Figure 29: Waveform acquired by Sentinel 3B over the Adda River. This waveform was acquired during cycle n°65, on April 16<sup>th</sup> 2022.



<b>ASSESSMENT OF CLOSED LOOP MODE PERFORMANCE AND FEASIBILITY OF AN OPEN LOOP MODE FOR SARIN MISSIONS</b>	Ref	NOV-FE-0747-NT-013		
	Issue	1	Date	21/03/23
	Rev	0	Date	21/03/23
	Page	36/36		

## 6. Conclusion

In this report, we have demonstrated some limitations of the CryoSat-2 SARin data in measuring inland water surface heights in heterogenous areas. Most of the results presented illustrate cases of unreliable height estimations from SARin data. However, it is important to note that CryoSat-2 provides accurate water height measurements in many other areas outside the Alps, which represents a worst-case scenario we knowingly studied. Using satellites to monitor inland water heights in such areas remains crucial: mountain lakes and rivers supply the rest of the downstream hydrographical network, the recession of glaciers and the decrease of snowfall are changing their dynamics, and they are located in areas that can be difficult to access for in-situ measurements.

**Our results show that implementing the OLTC on a SARin altimeter could enhance data acquisition for both lakes and rivers:** the incorporation of the DEM should help centering the radar’s reception window and significantly improve the results. Although the SARin instrument on CryoSat-2 possesses slightly different characteristics compared to the altimeters currently using OLTC, it has its own set of advantages. For example, the SRAL instrument of Sentinel-3 A&B has a 60m wide reception window, while CryoSat-2’s SARin features a 240m reception window and can acquire data from objects located several kilometers across track. With effective waveform centering provided by the OLTC, the SARin can detect various objects near the water body of interest. While the results might not be as optimal as those from Sentinel-3 or Jason-3, where over 90% of water bodies coded in the OLTC are detected, **CryoSat-2’s exceptionally dense coverage of the Earth’s surface, in contrast to other altimetry missions, offers the potential to monitor a vast number of water bodies.**

Addressing memory issues may present a challenge when implementing the OLTC on a satellite similar to CryoSat-2. The OLTC tables are currently sampled under the trajectory of the satellite, with a frequency of approximately 1 point per kilometre. Therefore, the memory space they require is directly dependent on the number of orbits per cycle. Sentinel-3 A&B satellites have 385 orbits per cycle, and Jason-3 and Sentinel-6 127, while Cryosat has 5344 orbits per cycle, and future altimetry missions like CRISTAL may have a similar number of orbits per cycle [RD14]. The potential of the dedicated DEM is then far beyond what is embarked on the missions currently using the OLTC. In order to implement the OLTC onboard future SARin missions, actions to save memory usage should be considered: the compression of the DEM, as it is currently performed with the Jason-3 and Sentinel-3 A&B OLTC tables; or for instance the splitting of the OLTC tables into parts that can be loaded on board, combined with a mechanism allowing the satellite to load the next OLTC subset when it has finished reading the previous one.

Finally, we have demonstrated the potential benefits of using the OLTC for SARin in mountainous regions. While this study has not yet confirmed the OLTC’s ability to address the phase wrapping issue, which is another phenomenon specific to interferometric synthetic aperture radars, it does provide a foundation for further exploration and studies in this area. This progress represents a promising step toward overcoming challenges and enhancing the capabilities of the SARin instrument in various landscapes.